IN-20
175562
P.52

NASA Contractor Report 191155

The PIT MkV Pulsed Inductive Thruster

C. Lee Dailey
TRW Space & Technology Group
One Space Park
Redondo Beach, California

and

Ralph H. Lovberg
University of California
San Diego, California

Prepared for
Lewis Research Center
Under Contract NAS1-19291

July 1993

NASA
National Aeronautics and
Space Administration

The PIT MkV Pulsed Inductive Thruster

C. Lee Dailey
TRW Space & Technology Group
Redondo Beach, California 90278

and

Ralph H. Lovberg
University of California
San Diego, California 92037

Summary

The pulsed inductive thruster (PIT) is an electrodeless, magnetic rocket engine that can operate with any gaseous propellant. A puff of gas injected against the face of a flat (spiral) coil is ionized and ejected by the magnetic field of a fast-rising current pulse from a capacitor bank discharge. Single shot operation on an impulse balance has provided efficiency and I_{sp} data that characterize operation at any power level (pulse rate). The 1-m diameter MkV thruster concept offers low estimated engine mass at low powers, together with power capability up to more than 1 MW for the 1-m diameter design. A 20 kW design estimate indicates specific mass comparable to Ion Engine specific mass for 10,000 hour operation, while a 100,000 hour design would have a specific mass 1/3 that of the Ion Engine. Performance data are reported for ammonia and hydrazine. With ammonia, at 32 KV coil voltage, efficiency is a little more than 50% from 4000 to more than 8000 seconds I_{sp}. Comparison with data at 24 and 28 kV indicates that a wider Isp range could be achieved at higher coil voltages, if required for deep space missions.

Introduction

Principle of PIT. - The pulsed inductive thruster (PIT) concept has been studied for a number of years, and has given results that have been encouraging for its application to primary propulsion in interplanetary missions (1). It consists of a flat spiral induction coil, typically one meter in diameter, over which a propellant gas is transiently injected, and through which a strong pulsed current is passed when the propellant is optimally distributed over its surface. The azimuthal electric field associated with the rising magnetic field breaks down the gas, creating a plasma current ring that is repelled axially from the primary current of the induction coil. Propellant injection is depicted schematically in Figure 1, and the configuration of ionized propellant and accelerating magnetic field is shown in Figure 2.

It may be concluded from a comparison of the desired range of plasma velocities (10 to 80 km/s) and the physical size of the accelerator, particularly the distance over which the plasma current ring decouples from the primary coil (10-20 cm) that the characteristic pulse time in this device is a few microseconds. The PIT MkVa described in this paper typically stores 4000 Joules of energy, applies 32 kilovolts around the one-turn coil, and accelerates from 0.6 to 10 milligrams of propellant per shot.

A particular characteristic of any pulsed device is that its mass tends to be proportional to energy per shot rather than to average power. Hence, the specific mass of the thruster (kilograms per kilowatt) is inversely proportional to the pulse repetition rate, while specific impulse and efficiency are parameters of individual shots and hence independent of pulse rate. The mass of a PIT such as that described here is in excess of 100 kg. If operated at an average power of 20 kW, with a 10^5 hour lifetime, for example, the specific mass would be 8 kg/kW, and the pulse repetition rate approximately 6 Hz.

Advantage of the PIT Concept. - The PIT has two significant advantages over other thruster concepts. The first is greatly reduced erosion of thruster components by the plasma. Since the plasma current is produced by induction, the system has no electrodes. While the plasma is created initially against the insulating surface over the coil, it is lifted away from the insulator by the first current flow, and is out of physical contact thereafter. The main channel for energy flow from plasma to thruster is radiation; however, the plasma is of relatively low density, and provides insufficient radiant flux to the coil cover to create observable damage. The glass insulator over the coil of an earlier thruster was not observably affected after several tens of thousands of discharges. While this is encouraging, further work will be needed to verify the very low erosion that will be needed for the coil cover of a practical thruster.

The second advantage is that it is possible to operate the PIT directly from turbo-electric power supplies of present design without the need for voltage change and the associated mass of transformers. The thruster design described later in this paper employs a Marx connection of its energy storage capacitors in order to make the total voltage around the coil an integer multiple of the capacitor charging voltage. Thus, a desired coil voltage of 32 kV could be achieved with a four segment Marx loop with the capacitors directly connected to an 8 kV nuclear electric generator. The present thruster employs a two-segment Marx connection, and has been operated up to 32 kV coil voltage.

MkV Design

Background: Earlier Thrusters.- Design of the thrusters PIT MkV and MkVa was guided by results obtained from earlier devices in this series, particularly MkI and MkIV. The former employed coil voltage of 15 to 22 kV, and accelerated masses of 10 to 20 mg to Isp of 1500 to 2000 s at efficiency of approximately 30% (Ref. 2).

MkIV employed an induction coil of smaller diameter (0.6m rather than the standard 1m), and was configured to allow diode clamping of the capacitor bank in order to avoid voltage reversal (Ref. 3). It produced surprisingly low efficiency and Isp that were ultimately explained by a computer simulation of the plasma breakdown process in a model that included actual circuit elements of the thruster. A principal determinant of efficiency was found to be the circuit inductance external to the coil itself. Initial plasma formation over the coil reduced its reflected terminal inductance; the effect of excessive external inductance between the coil and bank is then to lower the coil voltage by inductive division to such an extent that the remaining azimuthal field in the propellant is incapable of ionizing it completely. Rigorous minimization of "parasitic" inductance is clearly an important design requirement.

Mission Requirements. - In recent years, interplanetary missions have become clearly identified as those for which moderate to high-power electric propulsion offers the most significant benefits. Accordingly, optimum Isp is in the range of 4000-8000 s, so that the parameters of MkI, for example, are no longer appropriate. The propellant velocity must at least be doubled, and for the same energy, its mass reduced by a factor of four or more. This translates also into doubling of voltage applied to the plasma, and reduction of capacitance by a factor of four.

The final design described below incorporates the above criteria. An initial version was designed and tested (as PIT MkV) with a 2000 joule bank. Its upgraded successor, PIT MkVa (4000j), has been the more successful design, and is described in what follows.

Electrical Circuit. - Rather than using charge voltage in excess of 30 kV, it was decided to employ the Marx-generator scheme discussed earlier in which each of the parallel one-turn strands of the complete coil is broken into two half-turn segments that have series capacitors connected between them. The circuit of a single strand is shown in Figure 3. Each capacitor C has one side grounded, and they are charged in parallel to voltage V_o; when the switches are closed, an emf of $2V_o$ appears around the circuit. The circuit is equivalent to a full-turn loop connected to a capacitance C/2, charged to $2V_o$. This scheme may be extended to any number n of series coil segments, so that for charging voltage V_o, an emf of nV_o will be applied around the full coil. For example, 30 kV coil emf would be produced with 3, 10 kV capacitors per turn of the coil. This connection scheme has no effect on coil or capacitor mass for a given energy.

Figure 4 shows schematically the nine parallel circuits that constitute the full coil. Each strand in the figure represents four physical strands connected in parallel. It is noted in Figure 3 that the quarter-turn spiral segments of the coil are placed alternately on the front and rear surfaces of an insulating support plate. They are connected together at the inner diameter (0.4 m), and to the coaxial feed lines from the capacitors at the outer diameter (1.0m). The spirals are configured to provide a uniform surface current density J_θ over the entire coil surface, except for the outer 5 cm, where J_θ is increased by a factor of 1.5 in order to compensate for edge losses of magnetic field strength.

The strands are photo-etched from 0.020" copper sheet, which is two skin depths thick at the unloaded oscillation frequency of the thruster circuit; this provides the lightest possible coil for a given material, consistent with minimum resistance. Strand width is 0.6 of the normal interval between strands, which leaves ample turn-to-turn insulation, while keeping the parasitic inductance between strands negligible. Figure 5 shows the completed coil prior to its installation in the thruster.

Each of the 18 capacitors has a capacitance of 2μF, and a maximum charge voltage rating of 20 kV,

although 16 kV has been the maximum used in the present series of experiments. In the Marx connection, the bank thus has an effective capacitance of 9μF, and a voltage of 32 kV, for an energy of 4600 Joules. The total inductance of the circuit is 740 nH.

Reduction of Parasitic Inductance. - External inductance of pulse circuits is mostly that of capacitors and switches, provided that care has been taken in the design of connecting transmission lines. Capacitors tend toward a lower limit of approximately 50 nH per unit, while a well designed high voltage gap switch will contribute the order of 10 nH. The single available strategy for significantly lowering the inductance contribution of these components is to parallel them in as large numbers as is feasible.

In PIT MkVa, nine four-strand circuits are operated in parallel. Each capacitor is separately switched, so that the cumulative inductance of the spark gaps does not exceed 3 nH. Together, the total inductance of the capacitors, spark gaps, and transmission lines is slightly over 25 nH.

The 6 mm gap between the front and rear coil spirals occupied by their acrylic support plate contributes 21 nH of parasitic inductance, and the 1.6mm glass cover plate over the front surface of the coil adds another 11 nH. Thus, the cumulative parasitic inductance is calculated to be approximately 60 nH.

Switches and Transmission Lines – The capacitors have a double-ended configuration, so that the spark gaps may be placed at the rear of the thruster and opened easily for inspection. This mounting also allows one of the gap electrodes to be grounded, and circumvents the need for high voltage blocking of the trigger lines. The gaps are of three-electrode "swinging cascade" design, having symmetrical electrode spacing and trigger biasing.

Four coaxial cables of 40 cm length connect the forward end of each capacitor to four corresponding coil strands. The minimum length of these cables is dictated by two considerations:

- The grounded metal plate upon which the capacitors are mounted must be removed from the rear coil surface by a distance greater than the decoupling distance between the coil and its plasma load. - Otherwise, acceleration of the plasma will effectively stop when its separation equals the plate-coil distance.

- The major difficulty with a parallel-gap array is the extremely stringent requirement for simultaneity of firing. If two parallel gaps are separated by some short time t (the transit time of an electrical signal between them), then the firing of one gap earlier than the second by more than t will result in removal of voltage from the second before its trigger arrives, and it will never fire at all. The 40 cm separation of each capacitor and switch from the common load gives a value of t of about 5 nanoseconds, which is adequate for turn-on of all the gaps by the trigger generator[1].

The master pulse generator provides each of the 18 coaxial trigger lines a voltage step that rises to 30 kV in 5 nS. The lines are made sufficiently long that an additional doubling of the voltage occurs upon reflection of the wave from the initially open circuit at the gap. It has been found that with variable gap pressure, simultaneous firing of all gaps can be achieved from 5 kV to the full rated bank voltage.

Propellant Pulser. - The fast gas valve employed for injection of the propellant layer over the coil is the same as used on all thrusters since MkI. It is driven by a coil and permanent magnet arrangement essentially identical to that in a large audio loudspeaker. The ceramic coil form is brazed to a stainless steel diaphragm that rests against a 2-in. diameter O-ring separating a gas plenum chamber from the throat of the conical nozzle that is directed toward the thruster coil. Application of a current pulse to the coil from a 5-Joule energy storage capacitor opens the valve a distance of 0.5 mm in a time of 150 μS. The valve can be driven closed in an equal time. The valve and its annular conical nozzle are mounted on a central pylon at the axis of the thruster. The gas puff is directed downward and outward toward the coil surface in such a way that momentarily in its flow, it is distributed in a thin layer over most of the coil. A ring of glass plates at the outer perimeter of the coil acts as a flow barrier for the propellant, and helps establish a fairly uniform distribution at the time of a shot.

Thrust Balance. - The thruster is mounted to a platform that is supported from a main base by four vertical compressionally loaded flexure straps. Together they form an harmonic oscillator whose period increases with mass of the supported load,

---

[1] While neighboring circuits in MkV are not actually hard-wired into contact with one another, they are virtually so because of the large mutual inductance between them.

passing to infinity (collapse) for a certain critical mass. Just short of the critical mass, the effective restoring spring constant becomes very small, allowing sensitive detection of very small impulses applied to a massive object such as the PIT.

For example, with a period of 1 second, an impulse of 0.01 N-S applied to the 200 kG thruster produces a transient oscillation of the balance whose amplitude is measurable to the order of 5% accuracy. A caveat associated with these low limits, however, is that the laboratory environment must be particularly quiet.

Mechanical Design. – The main frame of the thruster is built from acrylic plates, which allow free circulation of magnetic flux behind the drive coil. The valve pylon is also acrylic. Capacitors are mounted on an aluminum plate that provides structural strength and rigidity as well as acting as a common ground plane for the system. The thrust balance, consisting of a pair of rectangular aluminum angle frames connected by four 1" x 5" x .050" steel flexure straps, is incorporated as an integral part of the thruster structure.

A 1" steel shaft passes transversely through the frame just above the thruster center of mass, and provides a lifting point for the portable crane used to move it in and out of the vacuum tank, as well as supporting it in its work stand outside the tank. Because of the proximity of the shaft to the center of mass, the thruster can be easily rotated on its stand between horizontal and vertical positions, as may be required.

The various umbilical lines connecting the thruster to its external supply sources are hung in flexible arcs between the wall feed-through fittings and the thruster so that their effect in damping the thruster balance or imparting spurious spring constants is minimized. The 18 trigger lines, each of 4 m length, are draped over and bound to a special A-frame fitted inside the tank behind the thruster.

Notwithstanding the total of 23 electrical lines and 5 gas lines connected to it, the Q of the thruster-balance oscillator is approximately 50, and requires the insertion of additional damping for convenience of use.

When in place in the vacuum tank, the thruster rests on a three-point mount; two cradles attached to the tank wall receive the forward extensions of the lower thrust balance frame, and a pad at the rear receives the tip of a leveling screw on the same frame. The screw can be adjusted from outside the tank by a sealed shaft.

The completed MkVa thruster is shown in Figure 6; Figure 7 gives a rear view of its installation in the vacuum tank.

Control and Data Acquisition System.- The various functions associated with operation of the thruster are computer controlled. The program allows a choice of operation of individual subsystems, or else automatic sequencing of all necessary procedures leading up to a shot.

Data are acquired through a number of A/D channels whose outputs are logged and processed to give indication of impulse, Isp, and efficiency immediately after each shot. These data, together with relevant thruster parameters, are archived on the computer hard disk.

Charge voltage for the main bank and valve and the valve-shot delay time, as well as calibration constants for the gas metering system and thrust balance, can be entered at the controller keyboard by the operator.

A detailed description of the control system is given in Appendix A.

Calibrations

Mass. - The mass increment injected over the coil is measured through observation of the pressure drop in the gas plenum behind the valve, and its associated plumbing. The plenum volume itself is measured by observing the change of pressure drop when a calibrated reference volume is added to that of the normal plenum system. The overall precision of the mass measurement is approximately 2%.

Impulse. - The impulse delivered during a shot is determined from a rapid sequence of displacement measurements of the thrust balance subsequent to the bank discharge, during which a peak-finding routine locates the first oscillation maximum. A reference displacement, taken just prior to the shot, is then subtracted, and the result multiplied by a calibration constant.

The calibration constant is determined from application of a known impulse to the thruster. This impulse is that of a dropped pendulum of soft clay that strikes a plate on the thruster axis at the bottom of its swing, without rebound. Since only the pendulum mass and its height change during the drop need to be known, this method is capable of good accuracy and repeatability.

Appendix B discusses this calibration and the particular environmental noise problem associated with it.

Cumulative Probable Error in h and I_{sp}. - In addition to the probable errors in mass and impulse (Appendix B) calibrations, the main bank capacitance and voltage are each measured to approximately 1% accuracy.

Consequently, exclusive of the data scatter from thrust stand seismic noise, thruster efficiency measurements should be accurate to slightly less than 4%, and those of I_{sp} to approximately 2.5%.

Propellant Distribution. - Because of its ready availability, easy storability, and ease of handling, ammonia has been given major emphasis as the PIT propellant. Hydrazine is also an attractive candidate, because it is used aboard spacecraft in other applications and the technology for its storage and handling is well established. For these experiments, a mixture of dissociation products (N_2 + 4 NH_3) has been employed. A drawback to the use of hydrazine is that the heat released upon its dissociation in the thruster adds to the overall thermal power that must be radiated.

It is necessary for efficiency of the thruster that the injected propellant increment be well placed over the coil at the time of a shot. The gas ideally should be uniformly spread over the coil area, and in a layer that is thin compared to the effective acceleration stroke (7.5 cm).

Measurement of the distribution of propellant is accomplished by use of a fast ionization gauge probe made from the elements of a miniature pentode vacuum tube (CK5702 or 6AH6), according to the scheme of J. Marshall (Ref. 4). Figure 8 is a set of four time-sequential contour maps of the injected mass density over the thruster coil, obtained by mapping of a 48-point grid in the r-z plane. Each graph covers the radial interval from 25 cm to 50 cm (the coil spans 20 to 50 cm), and an axial interval of 0 (coil surface) to 12 cm. Gas incident from the conical nozzle flows downward and to the right from the upper left corner of the frame.

Compression of the flow against the coil, and subsequent outward flow toward the confining cuff are evident in the figures. While the compression of the gas against the coil appears tightest in the 0.9 ms frame, there is still a substantial inflow from the nozzle, so that firing at that time would leave a significant portion of the total injected mass behind. 1.1ms (the fourth frame) has been found to give the best efficiency. Figure 9 is a 3-dimensional surface representation of the same data set. The input flow channel is particularly well depicted as the large open area on the bounding z = 11 surface between r = 25 and r=35 cm. Note that while this input flow has dropped significantly at 1.1 ms, an axial outward flow away from the coil has begun between r=40 and r=50 cm.

Thruster Performance. - Measurements of efficiency (η) and specific impulse (I_{sp}) of PIT MkVa were made with ammonia propellant at bank voltages of 12, 14, 15, and 16 kV, and with hydrazine products (N_2 + 4 NH_3) at 12 and 14 kV.

Data Format. - In Figures 10-15 we present the results of five runs, taken at the propellant and voltage combinations given above. For each run, I_{sp} was varied by changing the injected propellant mass over the range of values listed on its η - I_{sp} plot. The solid curve on each plot is an approximate best fit to the data points; the dashed curve is generated by the PITV simulation program that has been used as a design guide for this series of thrusters, and is described in detail in Appendix C. The program has two adjustable parameters, the thickness of the injected gas layer on the coil surface at the time of firing (δ_m), and the resistivity of the plasma, or equivalently, the plasma electron temperature (T_e). An average value for δ_m can be deduced from probe measurements of the gas distribution; this value is assigned, and the temperature is then adjusted for a best fit to the data.

Data Scatter. - In the plots, each symbol denotes a particular value of injected mass. It may be noted that points within an individual mass group are scattered along a diagonal line. This scatter originates almost entirely from seismic noise in the thrust balance that originates (and is ubiquitous) in the laboratory building (cf. Appendix B). Its amplitude typically corresponds to impulse of .003-.005 N-s. The shaded band surrounding each data set covers the region of expected data scatter for a noise amplitude corresponding to .004 N-s impulse. Since η varies quadratically with impulse, and I_{sp} is linear, the scatter patterns of individual symbols lie along parabolas that are centered at the origin.

Discussion of Data

Ammonia. – Figures 10-13 are η-I_{sp} plots of data taken at 12, 14, 15, and 16 kV, respectively. In these and in the hydrazine data to follow, the simulation curves are fitted to the higher mass

points, which always exhibit the least seismic noise scatter.

These graphs reveal a characteristic trait of PIT behavior; it may be seen that the data in the lower voltage plots (12, 14 and 15 kV) generally follow the simulation curve toward higher I_{sp} until, at a certain critical low limit of injected mass, they break away and fall toward lower efficiencies as I_{sp} increases. The critical mass is a function of bank voltage. At 12 kV, it is approximately 2 mg, and at 14 kV, 1.5 mg, and at 15 kV, 1 mg. At 16 kV, it is apparent that the critical mass is less than the 0.69 mg of the lowest mass data.

The 16 kV data merit special attention. First, the excellent coupling to a mass as low as 0.7 mg has allowed the achievement of an I_{sp} of 8200 s with efficiency above 50%. It may also be noted, however, that above I_{sp} of 5000 s efficiency no longer increases.

The η-I_{sp} characteristic of the PIT passes through a maximum when an optimum match between the plasma transit time to decoupling and the electrical period of the oscillating pulser is achieved. If the transit time is too long, the plasma resistive loss grows in comparison to the work of acceleration; if the transit is too quick, decoupling occurs before the bank energy has been transferred to the plasma. While the efficiency loss in this instance has not become serious at 8000 s, the trend is apparent.

The plasma temperatures required to achieve a fit of the simulation curves to the data increase steadily with voltage, as would be expected, and also have values that are plausible for this level of plasma and current density.

Hydrazine. - In both of the hydrazine plots (Figures 14 and 15) the majority of data points are taken below the critical mass level. These runs do not allow a clear determination of the critical mass, because there is not in either case an extended region of conformation with the simulation curve.

It is evident, however, that for the same bank voltage, the hydrazine plasma achieves a lower temperature than ammonia, and so operates at lower efficiency.

Facility Effects. - The cumulative surface area of all components of the MkVa thruster is large; moreover, many of the thruster materials (epoxies, acrylics, etc.) are intrinsically poor vacuum materials. As a consequence, even a 12" diffusion pump is incapable of maintaining a better tank vacuum than about 0.2 millitorr. The tank is relatively small, so that only about one meter of free drift space lies between the thruster and the end wall. These constraints raise questions concerning distortion of data by such processes as inclusion of background gas into the injected propellant, or the application of secondary increments of impulse by gas returning to the thruster from the end of the tank.

It can be readily concluded that the addition of 0.2 micron pressure to that of the propellant against the coil (typically more than 100 microns) is not itself a serious change. Also, the propellant returning to the thruster from the end of the tank has been reduced to nearly room temperature by wall interaction, so its momentum is of the order of 1% of what it initially carried away.

More important is the possibility that between shots, a significant mass is adsorbed on the coil surface from the ambient background, and that this mass is all desorbed at the time of plasma formation and combined with the injected propellant for a single discharge. Equally serious might be the dislodging of an adsorbed gas layer from the end of the tank by the high velocity incident plasma. While this cloud would return with low velocity, its total mass might be large enough to impart significant additional momentum to the thruster.

We conclude, through a detailed analysis of experimental impulse data, that these effects are probably not important in the results presented in this report. That analysis is given in Appendix D.

Magnetic Field Mapping

Procedure. - Estimates of expected thruster performance made with the PITV simulation have incorporated the idealization that the propellant is uniformly distributed over the coil, and that all of the mass is accelerated by the first half-cycle of current oscillation. It is important to be able to test this assumption experimentally, especially in instances where performance of the thruster falls significantly below prediction.

As shown earlier, the initial mass distribution has been measured with the fast ionization gauge probe. For observation of the distribution of magnetic field and plasma current during the actual acceleration, we have employed a magnetic coil probe. At each of 72 points on a grid in the r-z plane that covers the acceleration space, a shot of the thruster results in a time series B_r (r,z,t) from the probe and its integrator that is recorded on a

digital oscilloscope and archived by the data acquisition computer. These records can subsequently be cross-plotted as field contour maps or 3-dimensional surface plots for selected times. The thruster exhibits the excellent shot-to-shot reproducibility required by this mapping technique.

The sampling grid near the coil is non-uniform in its point spacing. During the initial formation and early acceleration of the plasma current sheet, the field distribution changes rapidly along z, but very gently as a function of r. Thus, a small z interval is required for the grid points. As the plasma moves away from the coil, the current thickens, so that a coarser grid is adequate for its characterization. The grid is mapped as follows: (a) axial scans are taken every 5 cm in radius, from r=25 cm to r=50 cm, with b) each axial scan consisting of points every 5 mm from z=0 to z=3 cm, one point per cm from z=3 cm to z=8 cm, with a final point at z=10 cm. Each record from the probe is digitized as 512 samples, taken every 40 ns.

The 72 records for each data run are entered into a spreadsheet for initial processing, and then transferred, as 2-dimensional arrays for selected times to a plotting program for preparation as contour maps.

Results. - We present the magnetic field distributions for two conditions of the thruster. The first is for 2.4 mg of ammonia propellant at a bank voltage of 14 kV, where the efficiency is at maximum (52%) and Isp is about 4000 s (Figure 11). The second case is for 1 mg of ammonia at 12 kV, where the mass is below the critical value at which efficiency begins to drop significantly. Here, actual efficiency is 38%, where ideally, it would be about 48% (Figure 10).

Initially, a pair of probe traces (Figure 16) will illustrate some general characteristics of the 2.4 mg, 14 kV discharge. The first is the field record adjacent to the coil (z= 0.5 cm) and at a radius of 40 cm. Since there is not significant plasma current between the probe and coil at this position, the probe signal closely follows the total circuit current. The asymmetry of the I(t) curve between current onset and the first zero is indicative of the large fractional inductance change during acceleration of the plasma; such a shape is a definite and necessary signature of efficient acceleration.

The second trace in Figure 16 is taken at the same radius as the first, but 4.5 cm farther away from the coil. It can be seen that for the first 1.5 μs, the plasma current sheet shields the probe from the B_r field. After passage of the plasma, the two positions have approximately equal field strength until 5 μs, where they once again diverge; this separation is due to the formation of a new sheet of reversed plasma current against the coil. Between 5 and 12 μs, the acceleration process of the first half-cycle repeats itself, and at 12 μs, one may see the formation of a third current sheet on the coil.

The average velocity of the first current sheet in the interval between the two stations is 3 cm/μs, while that of the second is slightly over 4 cm/μs.

Figure 17 is a set of four contour maps of B_r for 2.4 mg and 14 kV. The 1 μs map shows the current layer still tight against the coil, while at 2 μs, it has moved away and thickened. In the 1 μs plot, the parallelism of the contours with the coil indicates that the design objective of uniform B_r over the coil has been well met[2]. The current sheet is thinnest, and the current density highest, at a radius of 35 cm, which is the location of the peak of the injected propellant density (Figures 8 and 9).

The maps for 5.8 and 6 μs show the formation of the second half-cycle current sheet over the coil surface. One may note that this sheet does not cover the entire coil, but is confined to radii greater than 35 cm. We tentatively conclude that in the r=35 cm region, coupling between the plasma and first current sheet is sufficiently good to sweep out all the propellant, whereas in the 40-45 cm region, where there is a minimum in propellant density, enough mass is left behind by the first sheet to provide a significant load for the second.

Figure 18 depicts the run with 1 mg of propellant and 12 kV bank voltage. Here, the first half-cycle current sheet is well formed only in the radial interval between about 33 and 42 cm; there is poor coupling to the propellant outside of 45 cm. The second half-cycle discharge is sharply confined to the region of 45 cm radius. While coupling to the plasma is locally good, the unloaded portion of the coil presents a very large parasitic inductance, which lowers the efficiency of acceleration. Although the exact apportioning of efficiency losses among these effects is not known, it is clear that the irregular current distribution is correlated with unevenness of propellant placement, and that the "critical mass" is probably that mass below

[2] The "ripple" in the contour lines near the coil (z=0) is an artifact of the interpolation scheme in the contouring program. The lines should actually be quite straight.

which the first current sheet no longer covers the whole coil. An important goal of further development of the PIT will be to make the propellant layer more uniform than it is at present.

Erosion: Spectral Measurements. - A conceivable limit on very long life of the PIT might be the gradual erosion of the insulator over the coil. Plasma is first formed against the insulator, and while it is moved away early in the current flow, there is a short period of direct contact. During the second quarter-cycle, when the driving current is returning to zero from its first peak, magnetic flux is being withdrawn back into the coil, and a small amount of plasma, bound to the field lines, is returned with it to the surface. The major transport of energy from the plasma to the coil is hard UV radiation; while the photon flux should not be capable of direct ejection of insulator material the heating caused by its cumulative absorption in high rep-rate operation could cause evaporative loss if materials were badly chosen.

A standard diagnostic for plasma erosion of glass or silica insulators is the spectral doublet from SiII at 4128 and 4130 Å. In pinch-effect discharge tubes these lines are usually visible, even if other impurities have been eliminated by good vacuum technique. We have made a search for these and other impurity lines that might be anticipated, such as Carbon and Oxygen. For a 1.3 mg, 14 kV discharge, results are:

1. Carbon and Oxygen spectra cannot be unambiguously identified above a continuum that peaks in intensity at each of the current maxima.

2. The SiII 4128 Å line is barely discernible above the continuum.

3. Nitrogen spectra are strong. The NII 4630.5 Å line is approximately 100 times the continuum level; it is stronger during the second half-cycle of current than during the first.

4. Hydrogen spectra are not detectable above the continuum.

The monochromator line of sight was normally toward the coil at a radius of approximately 40 cm.

There is no visible evidence of insulator erosion after several thousand discharges. The glass has retained its pristine shine, and there is no crazing, such as is usual on the interior surfaces of pinch discharge tubes. These results offer no assurance that such an insulator would remain unblemished after 10^{10} shots; however, they encourage the conclusion that erosion will not be a major engineering problem.

Critique of the PITV Simulation. - The PITV simulation was originally written to provide a guide for design of the thruster. It has been surprisingly successful in predicting general levels of thruster performance, even though the plasma itself is rather crudely modeled. The fits to experimental data shown in the data plots have been achieved using values of the adjustable parameters that would otherwise have been guessed beforehand.

However, there are features of actual thruster operation that are not included in the model, the most important of which is that, as seen in the previous section, separate current sheets are accelerated away from the coil surface on each half-cycle of the oscillating bank current. (The model assumes that all of the mass is carried by the first sheet.) The fraction of the total mass accelerated by current sheets subsequent to the first has not yet been determined for PIT MkVa, although data from MkI showed it to be small. The result of this multiple acceleration could be a slight increase in efficiency with respect to the simulation result, since the average value of the plasma-coil coupling coefficient during acceleration is larger than for the single-sheet case. This efficiency increase should tend to compensate for a decrease that can be associated with irregularities in the mass distribution actually achieved over the coil. Contrarily, in instances of sub-critical mass loading where the first current sheet does not fully cover the coil, the simulation will fail to predict real performance.

Development for Space Missions. - Performance demonstrated by the PIT makes it an attractive option for deep space nuclear electric propulsion missions. While adequate for single shot testing at room temperature, the uncooled, glass and epoxy performance model would require modification in three important areas. These are: coil, valve and pulser (capacitor/switch assembly).

Coil. - Thermal design of the coil is the most important structural design issue of the thruster. We estimate that approximately 10% of the total energy of each shot is absorbed by the coil cover surface as hard UV radiation from the plasma. Direct resistive losses in the conductors are small by comparison. A primary design approach is that the coil must act as its own radiator for this energy. This means that the thermal conductivity of the transmission lines connecting the coil to the capacitor bank must be made as small as possible,

consistent with keeping their electrical resistance adequately low.

Figure 19 shows the effect of thruster power on coil surface temperature for the one-m diameter Mark Va, with an assumed emissively of 0.75. The figure also indicates the power sources that might be developed for the different power ranges. The Topaz 1 generates 6 kW. Design studies are proceeding to examine the feasibility of increasing this to the 40 kW indicated for Topaz 2. The SP 100 generator is shown at its nominal 100 kW rating for electrothermal conversion, with the possibility of reaching 500 kW by using dynamic conversion. Advanced technology developments might extend the nuclear electric power range to 1.2 MW, which could be used by the Mark Va thruster operating at 300 pulses per second.

Also shown in Figure 19 is the coil construction that would be used for the different power ranges. Copper coil elements would be used for any power up to 500 kW. Higher powers would require Molybdenum. TRW has developed a commercially available polyimide (TRW-R-8XX) that would be used for coil construction for operation up to 100,000 hours at 300 C (40 kW continuous power). Zirconia would be used for powers above 40 kW, with copper up to 500 kW and moly up to 1.2 MW. The low thermal conductivity of zirconia makes it attractive to stand off the higher coil temperatures with moderate heat flow through the transmission line leads to the capacitor connections.

Valve. - A 20 kW engine operating at 6 shots per second would require a life of about 2×10^9 shots for 100,000 hours of thrusting. A valve of the present design was tested at a repetition rate of 20 per second to a life of 3×10^6 shots, when the stainless steel diaphragm developed a fatigue crack. This life might be substantially increased by improved fabrication techniques and a better material, such as Inconel. The present valve has proven to be reliable for the present mode of single shot testing where, through three models of the PIT over five years, it has probably accumulated not more than 10^5 shots.

We are considering an alternate valve concept that may be better suited for very long life operation. It is based upon a Stirling engine piston developed for a space based helium refrigerator having a 10 year life. The piston is flexure constrained and oscillates within a very close fitting, but non-contacting cylinder. The flexure operates below the fatigue limit for infinite life so that without surface contact of any kind in either seals or bearings, operation life is unlimited. In the valve concept, the piston is replaced by a flexure-supported, open ended, cylinder having an azimuthal slit equidistant from the ends. The cylinder could be kept in constant amplitude oscillation by a magnetic driver, so that gas would flow from within the cylinder through its slit and into the sonic throat of a radial nozzle at the middle of the oscillation, when the slit and throat were aligned. The pulse rate would be double the oscillation frequency. This approach could be used for a high power thruster operating at a few hundred pulses per second. For either single shot, or low power operation, the valve would be constrained at one extreme of its harmonic motion by a permanent magnet, from which it would be released by a short pulse of opposite applied field. Upon arrival at the other extreme of its path a half cycle later it would be magnetically captured and subsequently released for the next pulse. Design for very long life should be possible for this adaptation of the helium refrigerator piston.

Pulser. - The pulser comprises the bank of capacitors and the solid state switches that discharge them. The spark gaps used for single shot testing are ideal for that purpose in that the switch breakdown time is less than the time required for breakdown and ionization of gas near the coil surface, and for current sheet formation, but they are not suitable for continuous, long life operation. Solid state switches would be required to begin conduction within 50 ns of initiation, and be capable of a circuit current rise rate of about 10^{10} amperes per second. A recently developed, and commercially available device, the Mos-Controlled-Thyristor may be capable of meeting these requirements.

The ideal pulser design would be to integrate the switch element assembly with the capacitor pads to achieve small pulser volume and mass, in addition to low parasitic inductance. An alternative approach, that would be convenient for development work would have the solid state switch configured as a "plug in" replacement for the spark gap.

Polypropylene energy discharge capacitors, using all-film construction have been life tested to failures in the range of 10^{10} to 10^{11}, at pulse rates of several kHz. Energy storage density is 27.5 joules per kilogram for 0.95 survivability after 10^{10} shots (Ref. 5). Life testing at TRW with capacitor pads of this construction has shown that shot life increases as the inverse 20th power of voltage (Ref. 2). Since energy density is proportional to voltage squared, the value corresponding to a life on N shots is given by,

$$E=27.5x(10^{10}/N)^{1/10} \text{ joules/kG}$$

Engine Development. - Development of a 100,000 hour, 40 kW engine with a copper/polyimide coil could be accomplished in a 2 years period. Coil construction could be accomplished in 6 months, while the long life valve and solid state switch might require from 1 to 2 years. A great deal of capacitor life testing should be done, both at the pad level and with complete capacitors to establish survivability data with a high degree of confidence. Accelerated testing can be used to acquire life data in a short time. The capacitors for a 10 pps thruster operating 100,000 hours ($3.6x10^9$ discharges) could be life tested for 1,000 hours (42 days) at 1000 pps.

By adopting the Mark V spark gap switch and valve designs, the thruster could be ready for single shot performance testing in 6 months. The long life valve and switches should be designed for interchangeability with the Mark V components, so that change over would be possible at any time during development.

The estimated specific mass of a 40 kW PIT is plotted in Figure 20 as a function of operation time. For 10,000 hours thrust time, the specific mass is estimated to be 5.6 kg/kW. For 100,000 hours design life, this value has increased to 6.2, an increase of 11% due to capacitor derating required for a decade shot life increase. By contrast, the ion engine specific mass has increased about a factor of 3, from 8.5 to 29 for the 10 fold life increase.

Although design details have not been worked out for continuous operation engines, component masses can be approximated as shown in the following tables to provide a preliminary estimate of specific mass for low and high power engines at 10,000 and 100,000 hours of thrust time.

	10,000 Hour 40 kW Engine	100,000 Hour 40 kW Engine
Capacitors	104 kg	131 kg/kW
Switches	21	21
Coil and Leads	23	23
Valve	7	7
Valve Pylon	6	6
Structure	25	25
Total Mass	186	213
Specific Mass	4.7 kg/kW	5.3 kg/kW
Charger Specific Mass	0.9	0.9
Total Specific Mass	5.6	6.2

	10,000 Hour 1.2 MW Engine	100,000 Hour 1.2 MW Engine
Capacitors	147 kg	185 kg
Switches	29	29
Coil and Leads	49	49
Valve	7	7
Valve Pylon	29	29
Structure	38	38
Total Mass	299	337
Specific Mass*	0.25 kg/kW	0.28 kg/kW

* Power conditioner mass required for capacitor charging is ignorable for a high power alternator.

These estimated specific masses are small compared to power source values (of the order of 5 to 10 percent) which is a necessary condition for a high ratio of efficiency to propulsion system specific mass.

EMI. - The thruster duty cycle is very low, even at a pulse rate of 300 per second, (1.2 MW) it is about one part in one thousand. The communication system would either ignore out of range signal peaks for the discharge period of 3 microseconds, or it could be programmed to do so. EMI associated with charging transients could presumably be handled with conventional techniques.

Acknowledgments. - Design, fabrication and preliminary testing of the Mark V thruster was supported by the TRW Independent Research and Development (IR&D) program in 1991. Performance mapping of the Mark V (efficiency and Isp) for several propellants was carried out in 1991 and 1992 under NASA LeRC funding, with Michael LaPointe, Project Manager. Subsequent modification of the thruster to the Mark Va configuration, and the performance mapping of ammonia and hydrazine described in this report were funded by the 1992 TRW IR&D program.

References

1) C. L. Dailey and R. H. Lovberg, "Large Diameter Inductive Plasma Thrusters," AIAA Paper 79-2093, October 1979.

2) C. L. Dailey and R. H. Lovberg, "Pulsed Inductive Thruster Technology," AFAL TR87-012, April 1987.

3) C. L. Dailey and R. H. Lovberg, "PIT Clamped Discharge Evaluation," Final Report, AFOSR Contract F49620-87-C-0059, December 1988.

4. J. Marshall, Proceeding Second International Conference on Peaceful Uses of Atomic Energy, Geneva, 1958, Vol. 31, P. 341.

5. D. Tammage, Maxwell Laboratories, Private Communication.

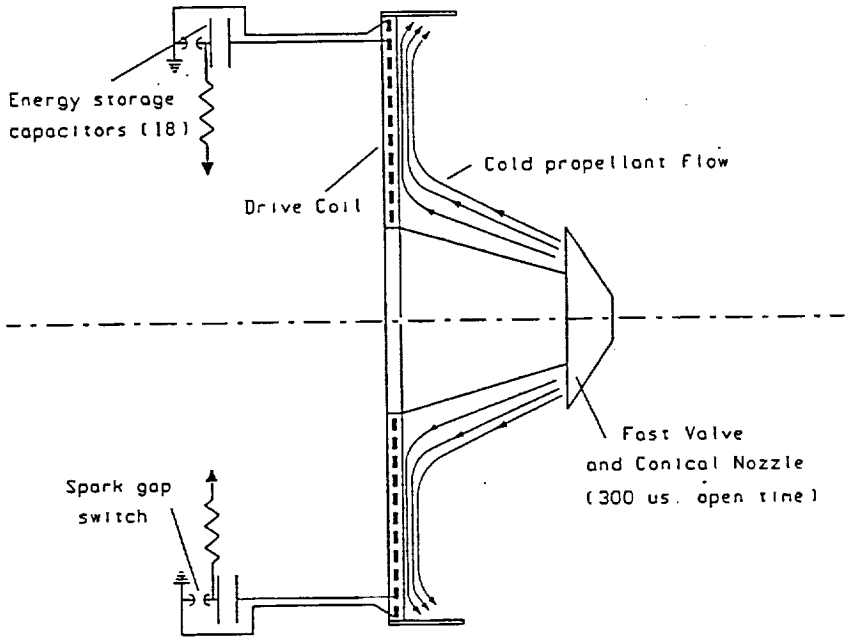

Figure 1. Propellant Injection Schematic

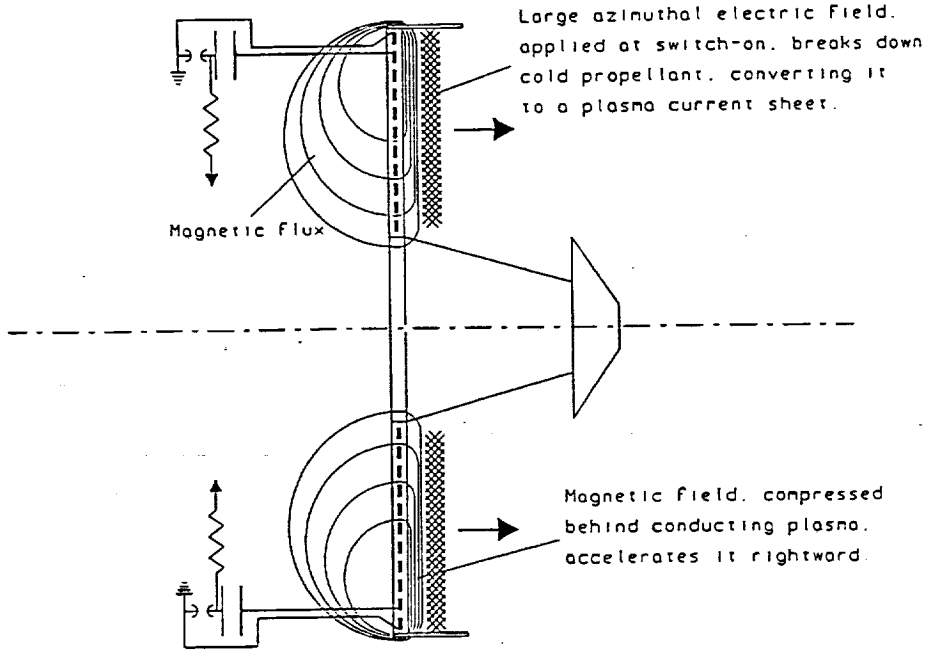

Figure 2. Magnetic Field and Plasma Current During Acceleration

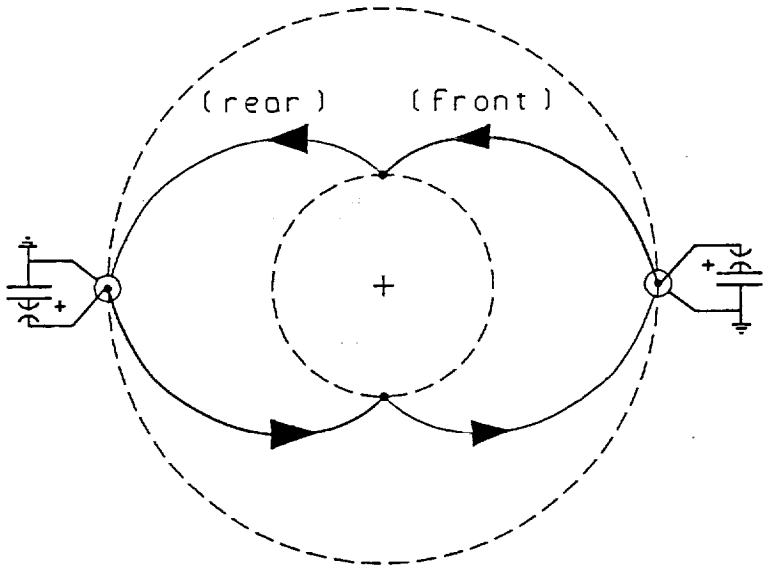

Figure 3. Single Coil Circuit Connections

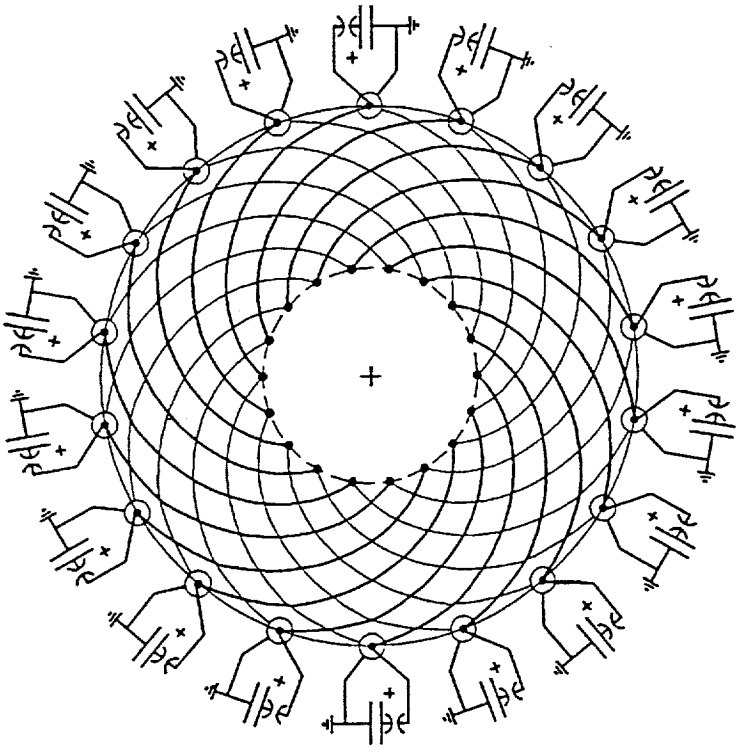

Figure 4. Composite Ciucuit for 18 Capacitors

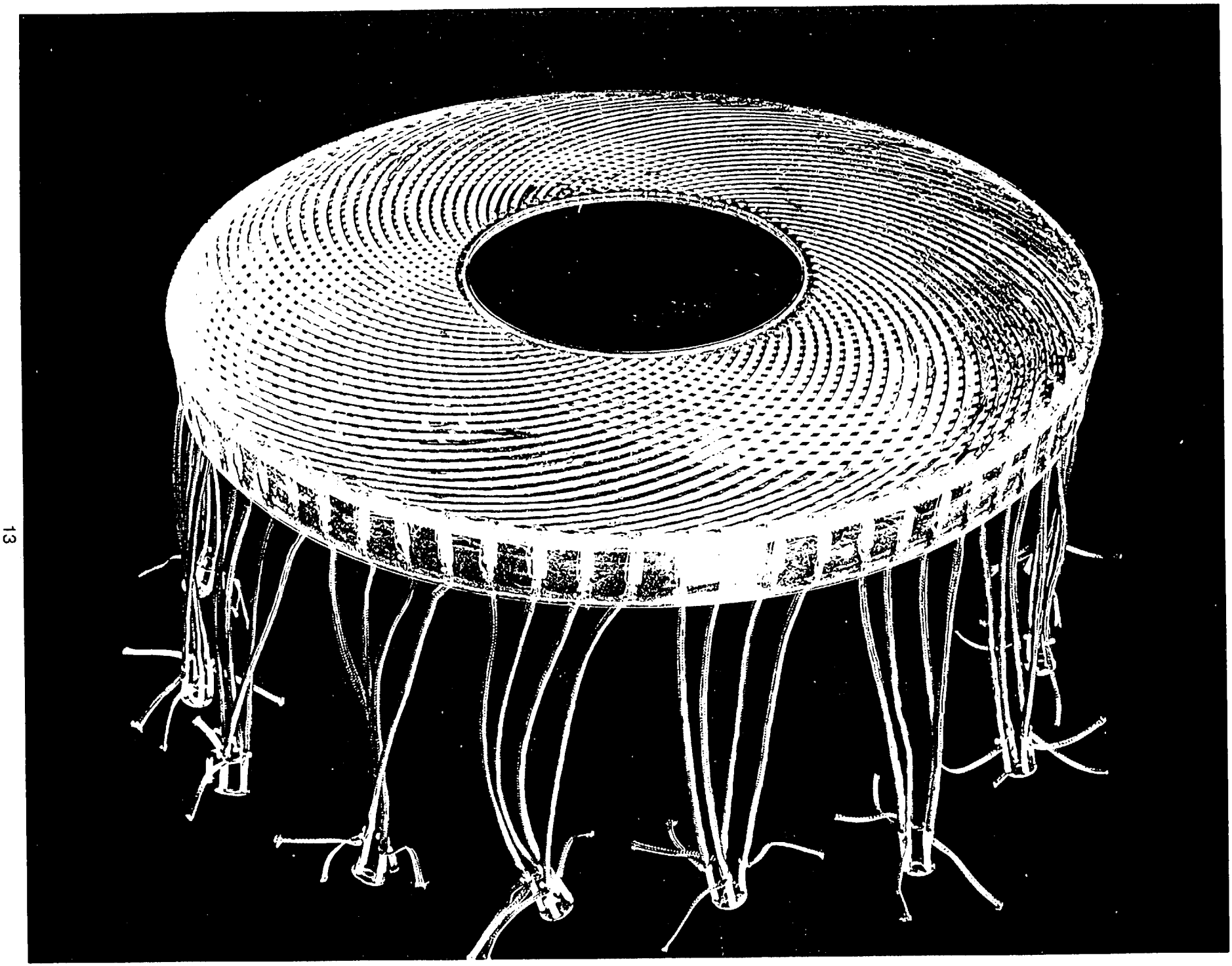

Figure 5. Coil and Lead Assembly After Impregnation

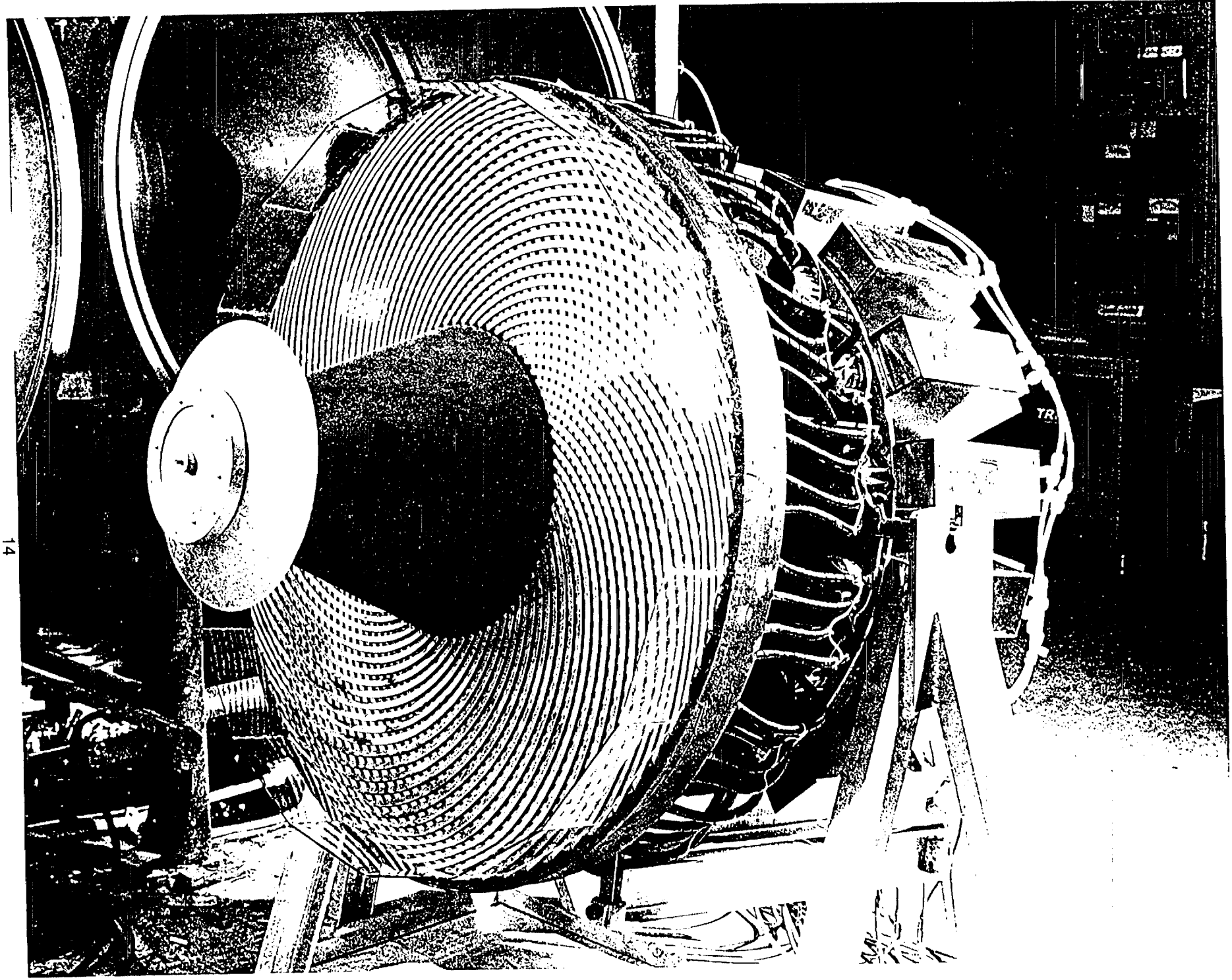

Figure 6. Mark Va Thruster on Work Stand

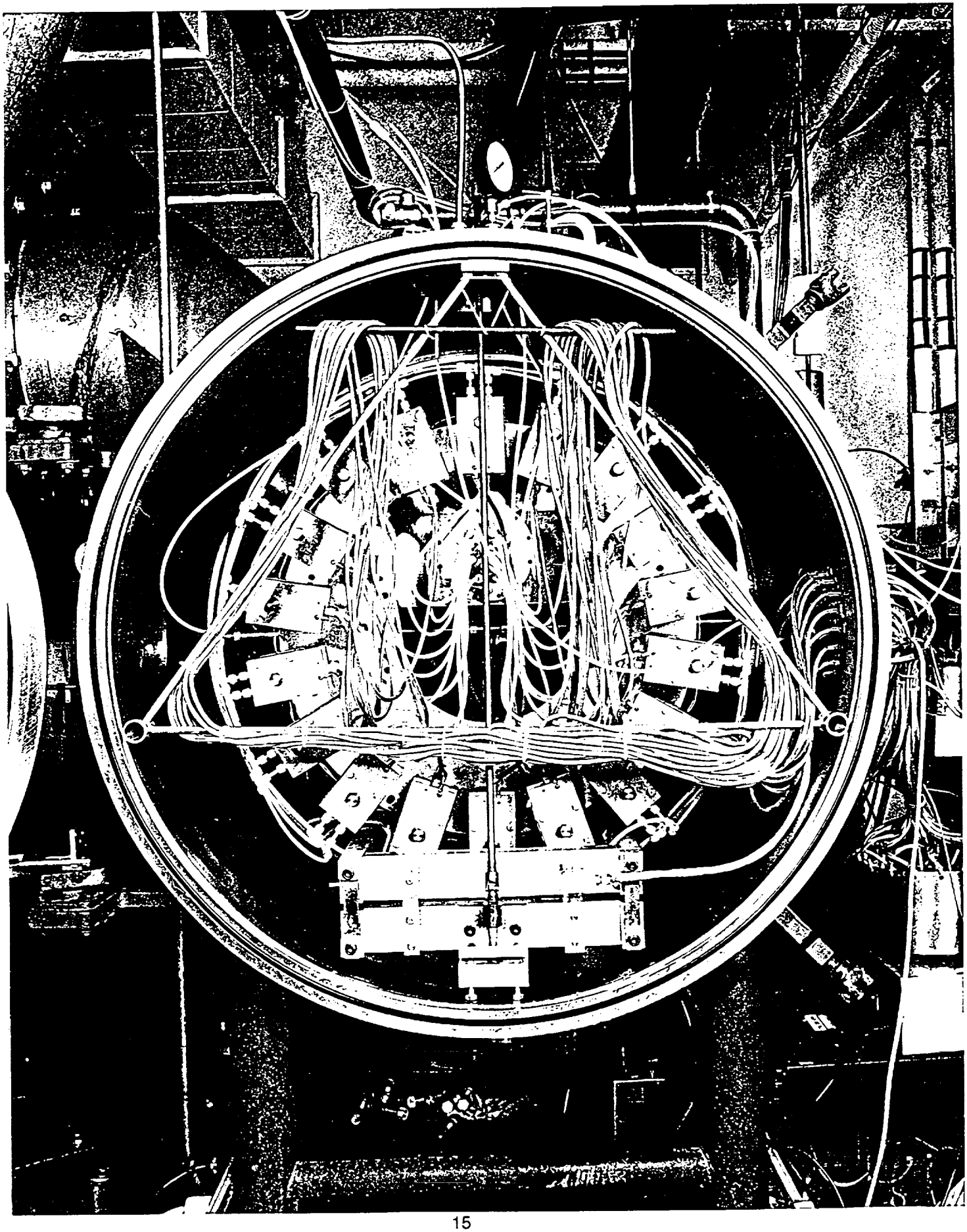

Figure 7. Rear View of Mark Va Thruster in 48" Vacuum Chamber

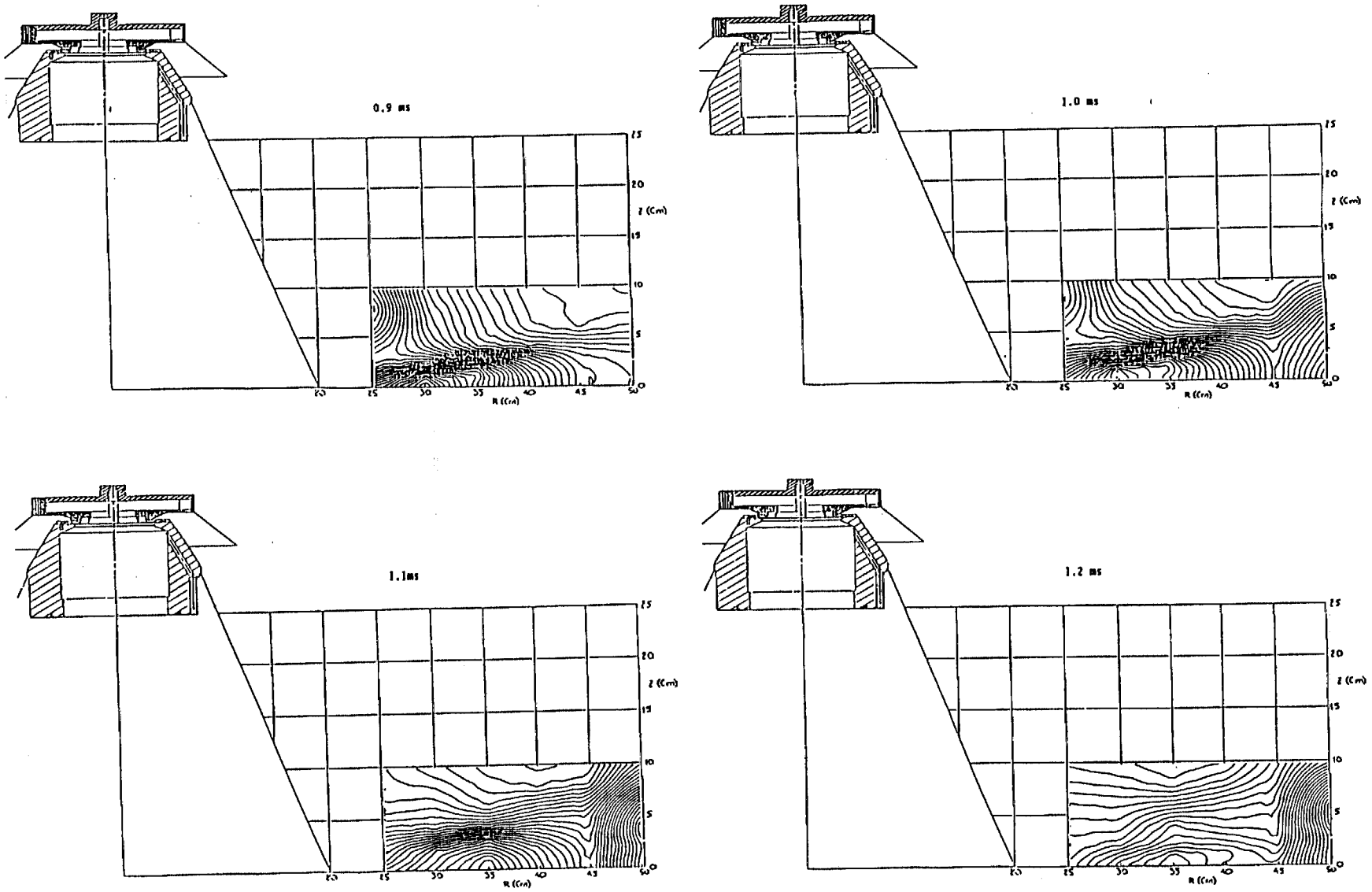

Figure 8. Gas Density Contour Maps at Different Delay Times

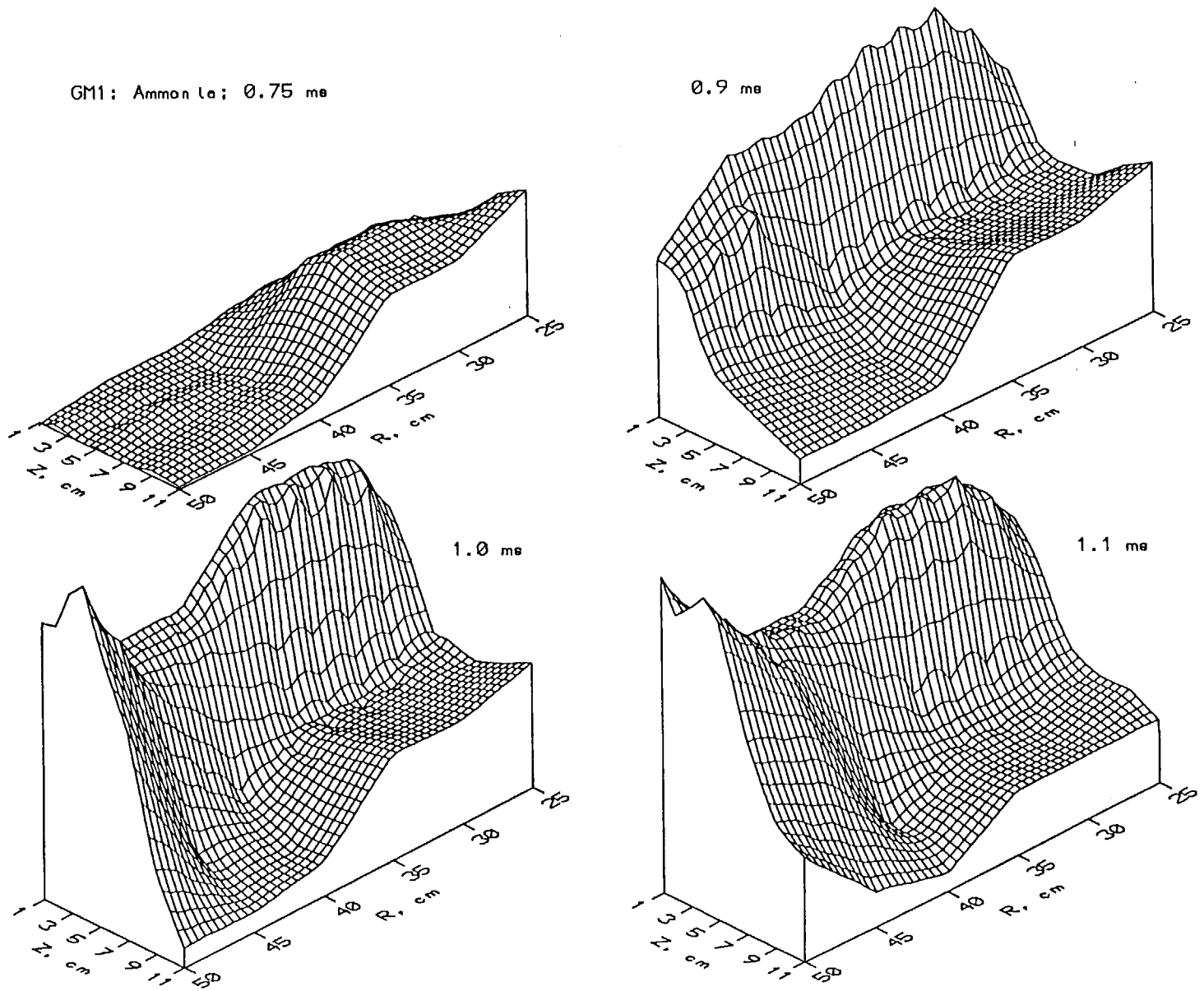

Figure 9. Gas Density Plots in Three Dimensional Form

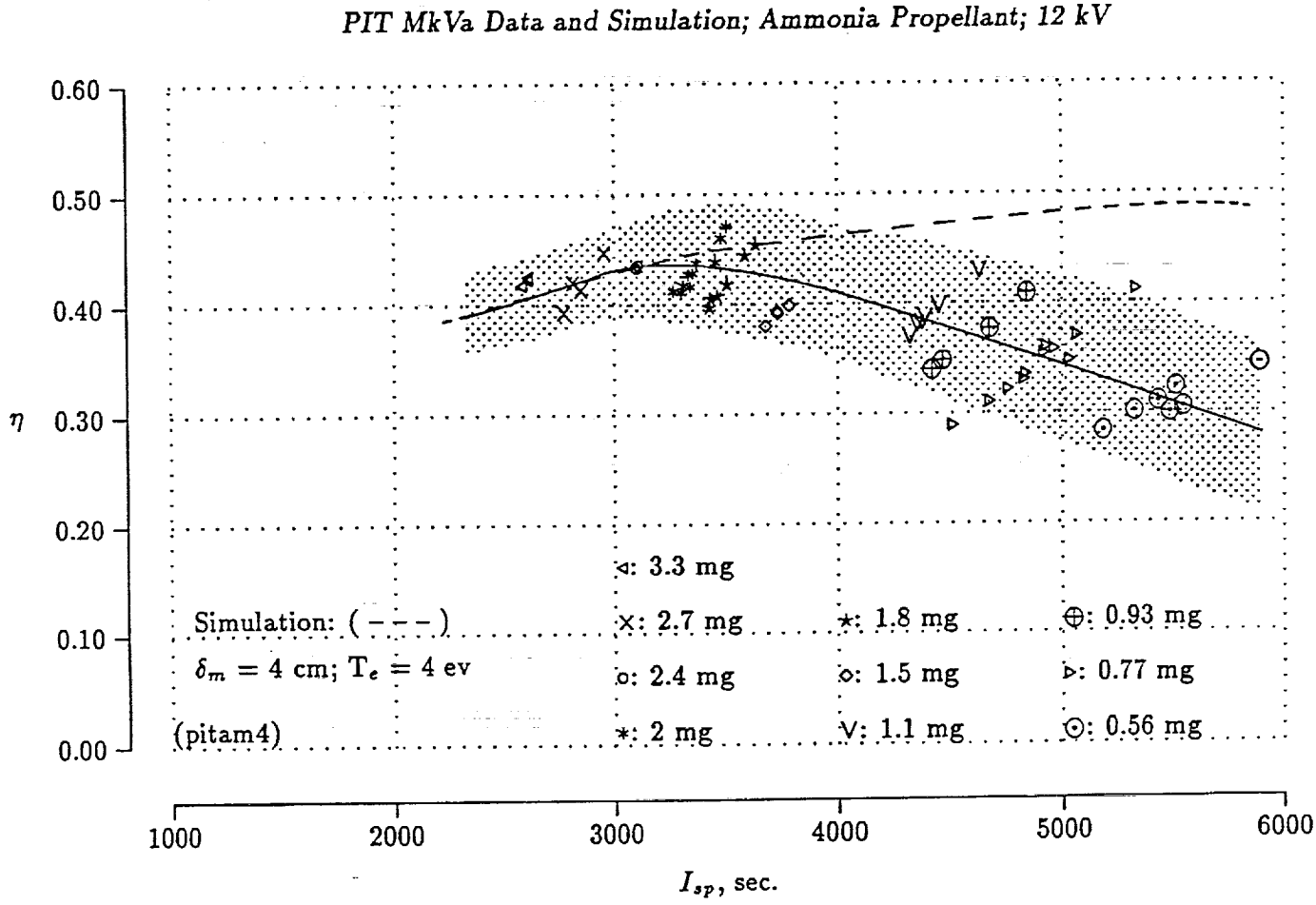
PIT MkVa Data and Simulation; Ammonia Propellant; 12 kV
0.60
0.50
0.40
0.30
0.20
0.10
0.00
η
Simulation: (- - -)
δm = 4 cm; Te = 4 ev
(pitam4)
◁: 3.3 mg
×: 2.7 mg
o: 2.4 mg
*: 2 mg
⋆: 1.8 mg
◇: 1.5 mg
V: 1.1 mg
⊕: 0.93 mg
▷: 0.77 mg
⊙: 0.56 mg
1000
2000
3000
4000
5000
6000
Isp, sec.

Fig.10

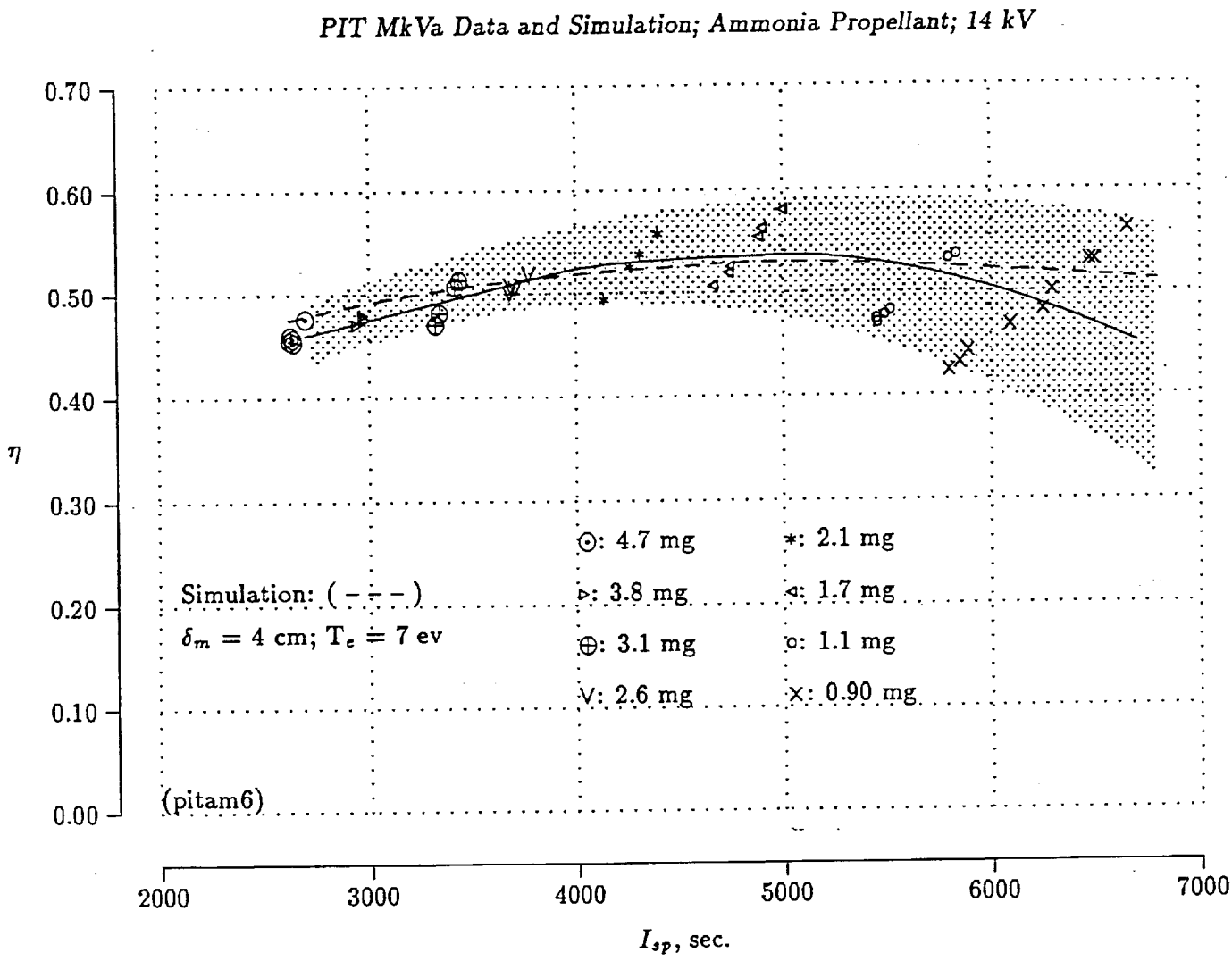
PIT MkVa Data and Simulation; Ammonia Propellant; 14 kV
0.70
0.60
0.50
0.40
0.30
0.20
0.10
0.00
η
Simulation: (– – –)
δ_m = 4 cm; T_e = 7 ev
⊙: 4.7 mg
▷: 3.8 mg
⊕: 3.1 mg
V: 2.6 mg
*: 2.1 mg
◁: 1.7 mg
o: 1.1 mg
×: 0.90 mg
(pitam6)
2000
3000
4000
5000
6000
7000
I_{sp}, sec.

Fig.11

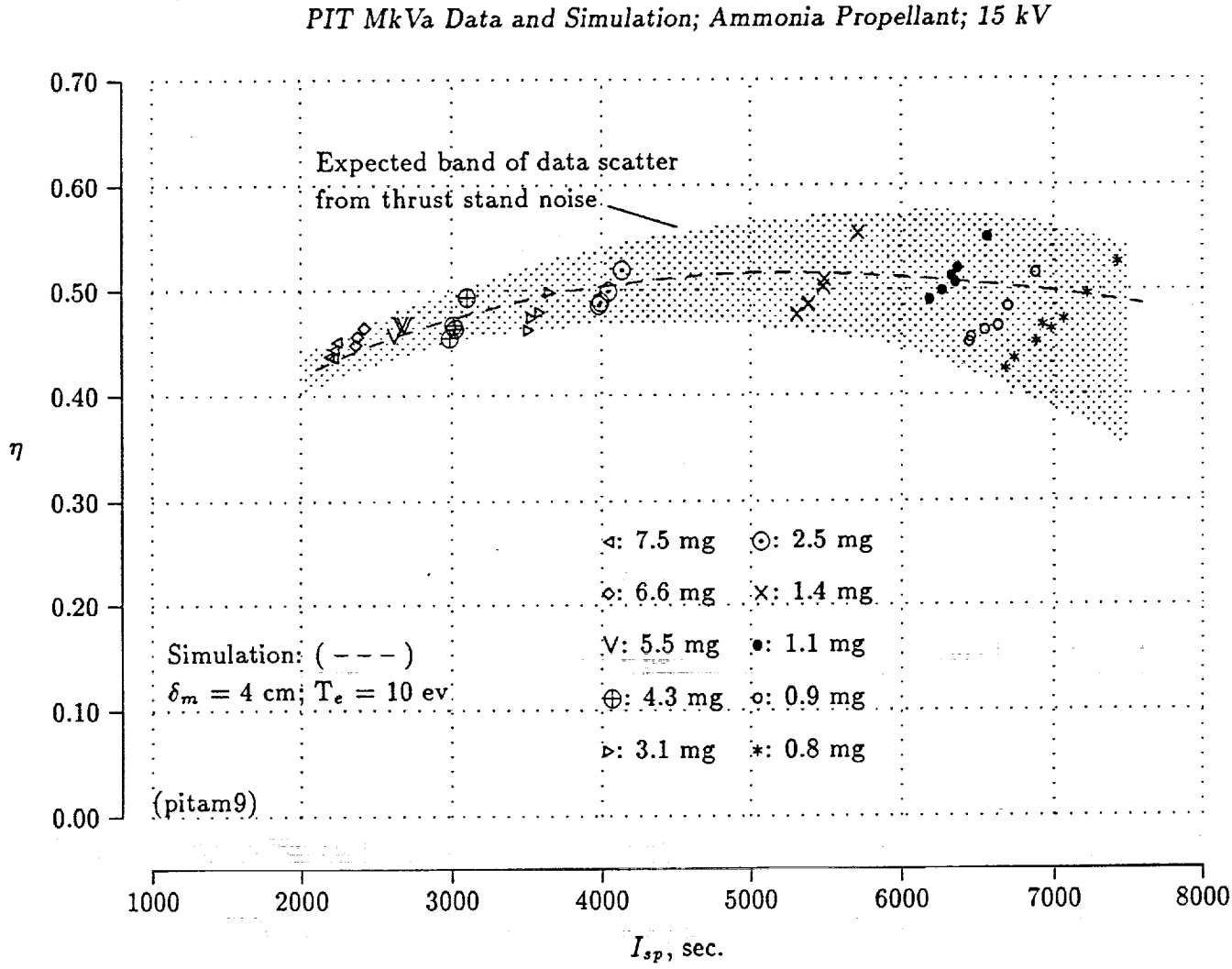
PIT MkVa Data and Simulation; Ammonia Propellant; 15 kV
Expected band of data scatter
from thrust stand noise
0.70
0.60
0.50
0.40
0.30
0.20
0.10
0.00
η
◁: 7.5 mg
⊙: 2.5 mg
◇: 6.6 mg
×: 1.4 mg
V: 5.5 mg
•: 1.1 mg
⊕: 4.3 mg
○: 0.9 mg
▷: 3.1 mg
*: 0.8 mg
Simulation: (- - -)
δ_m = 4 cm; T_e = 10 ev
(pitam9)
1000
2000
3000
4000
5000
6000
7000
8000
I_{sp}, sec.

Fig. 12

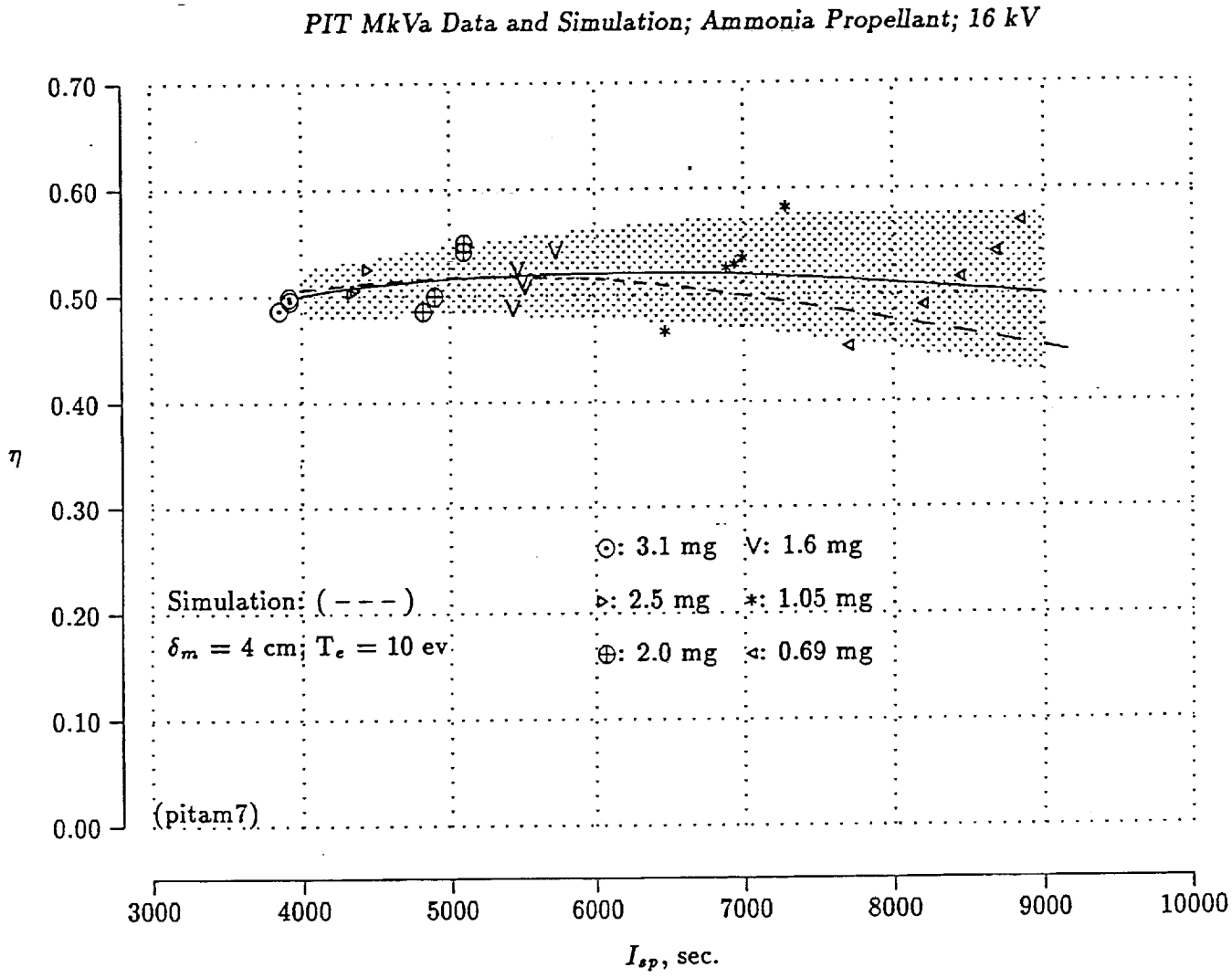
PIT MkVa Data and Simulation; Ammonia Propellant; 16 kV
0.70
0.60
0.50
0.40
0.30
0.20
0.10
0.00
η
Simulation: (- - -)
δ_m = 4 cm; T_e = 10 ev
⊙: 3.1 mg
V: 1.6 mg
▷: 2.5 mg
*: 1.05 mg
⊕: 2.0 mg
◁: 0.69 mg
(pitam7)
3000
4000
5000
6000
7000
8000
9000
10000
I_{sp}, sec.

Fig. 13

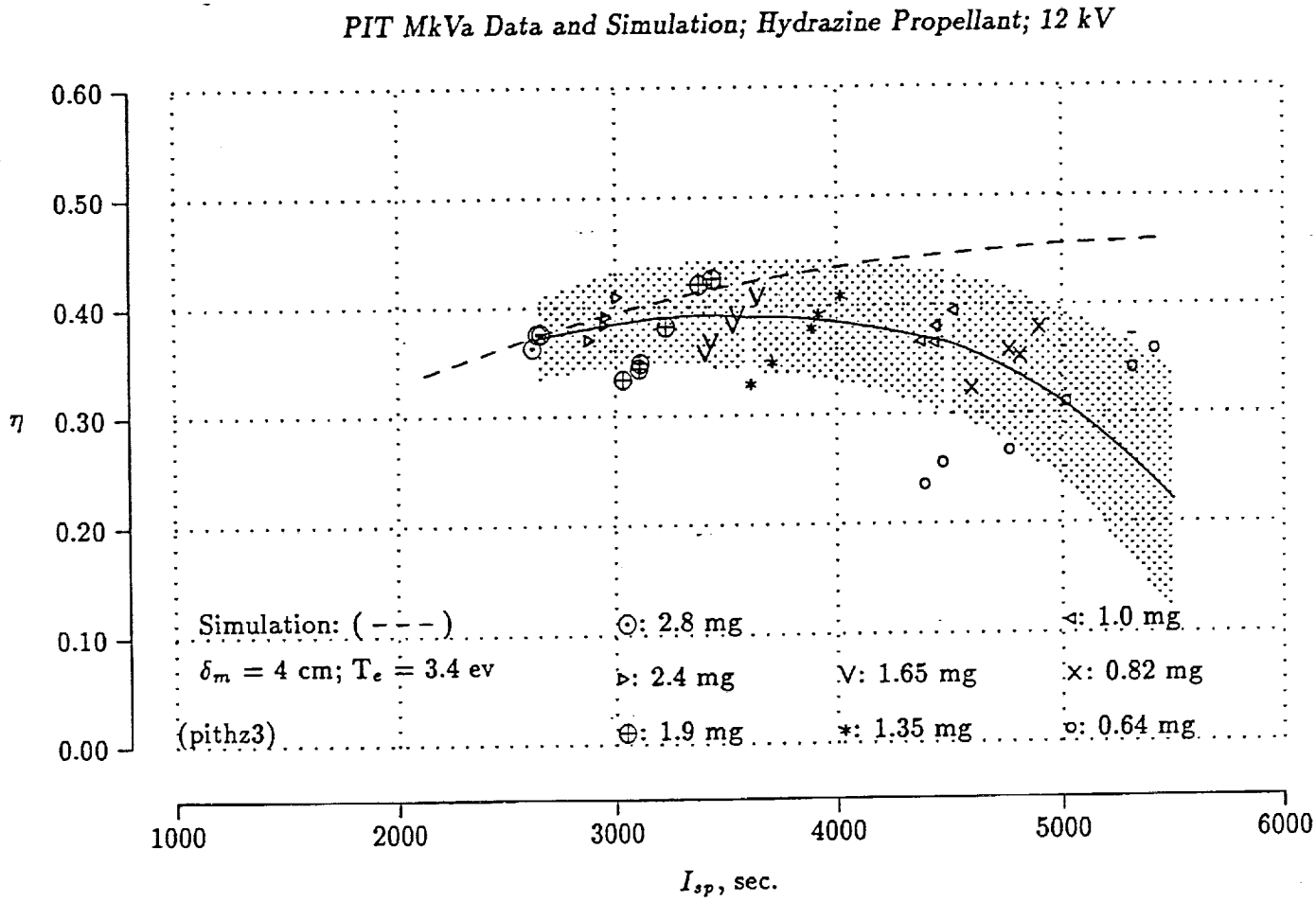
PIT MkVa Data and Simulation; Hydrazine Propellant; 12 kV
0.60
0.50
0.40
0.30
0.20
0.10
0.00
η
Simulation: (- - -)
δ_m = 4 cm; T_e = 3.4 ev
(pithz3)
⊙: 2.8 mg
▷: 2.4 mg
⊕: 1.9 mg
V: 1.65 mg
*: 1.35 mg
◁: 1.0 mg
×: 0.82 mg
○: 0.64 mg
1000
2000
3000
4000
5000
6000
I_{sp}, sec.

Fig. 14

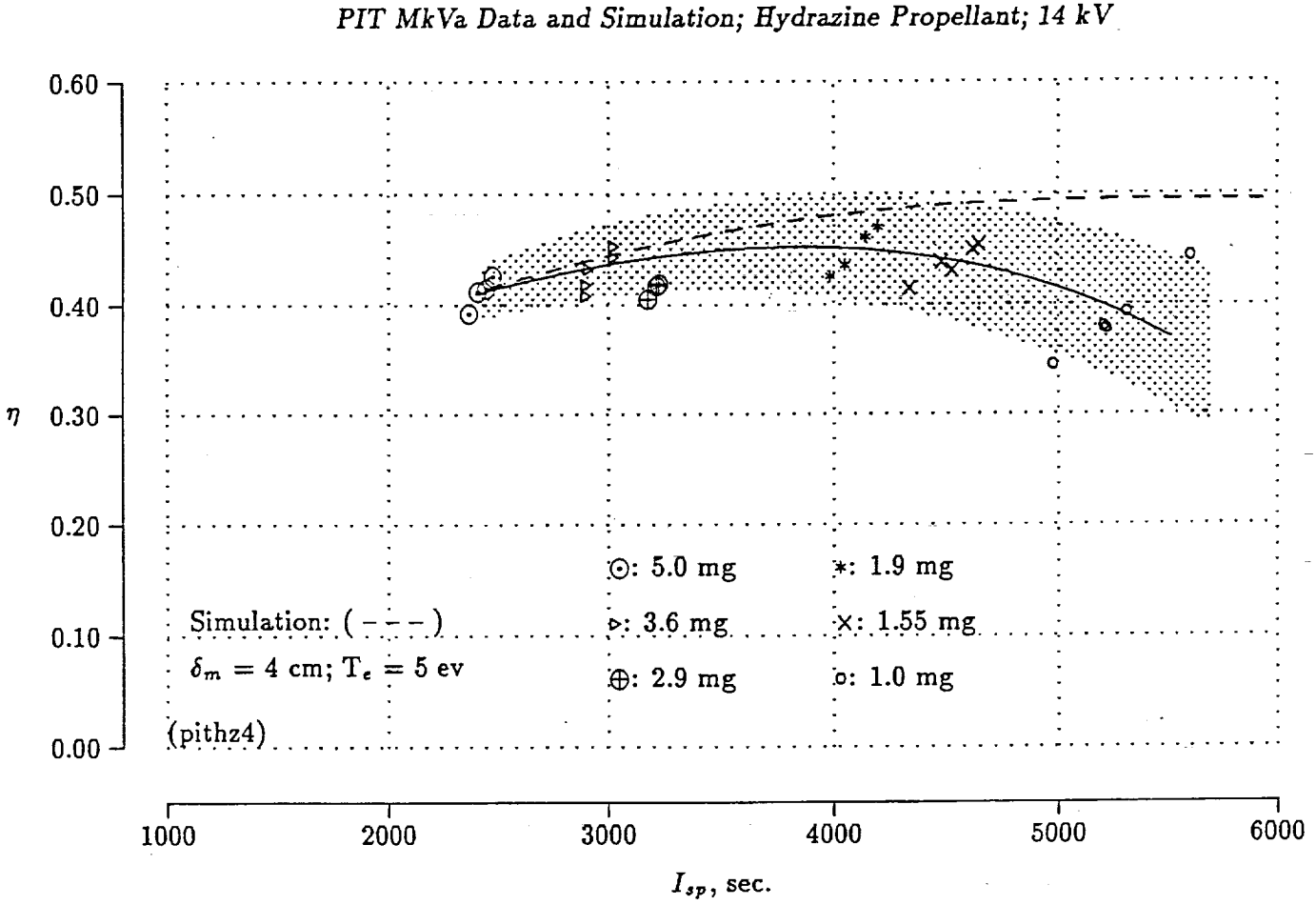
PIT MkVa Data and Simulation; Hydrazine Propellant; 14 kV
0.60
0.50
0.40
0.30
0.20
0.10
0.00
η
Simulation: (– – –)
δ_m = 4 cm; T_e = 5 ev
(pithz4)
⊙: 5.0 mg
▷: 3.6 mg
⊕: 2.9 mg
*: 1.9 mg
×: 1.55 mg
○: 1.0 mg
1000
2000
3000
4000
5000
6000
I_{sp}, sec.

Fig. 15

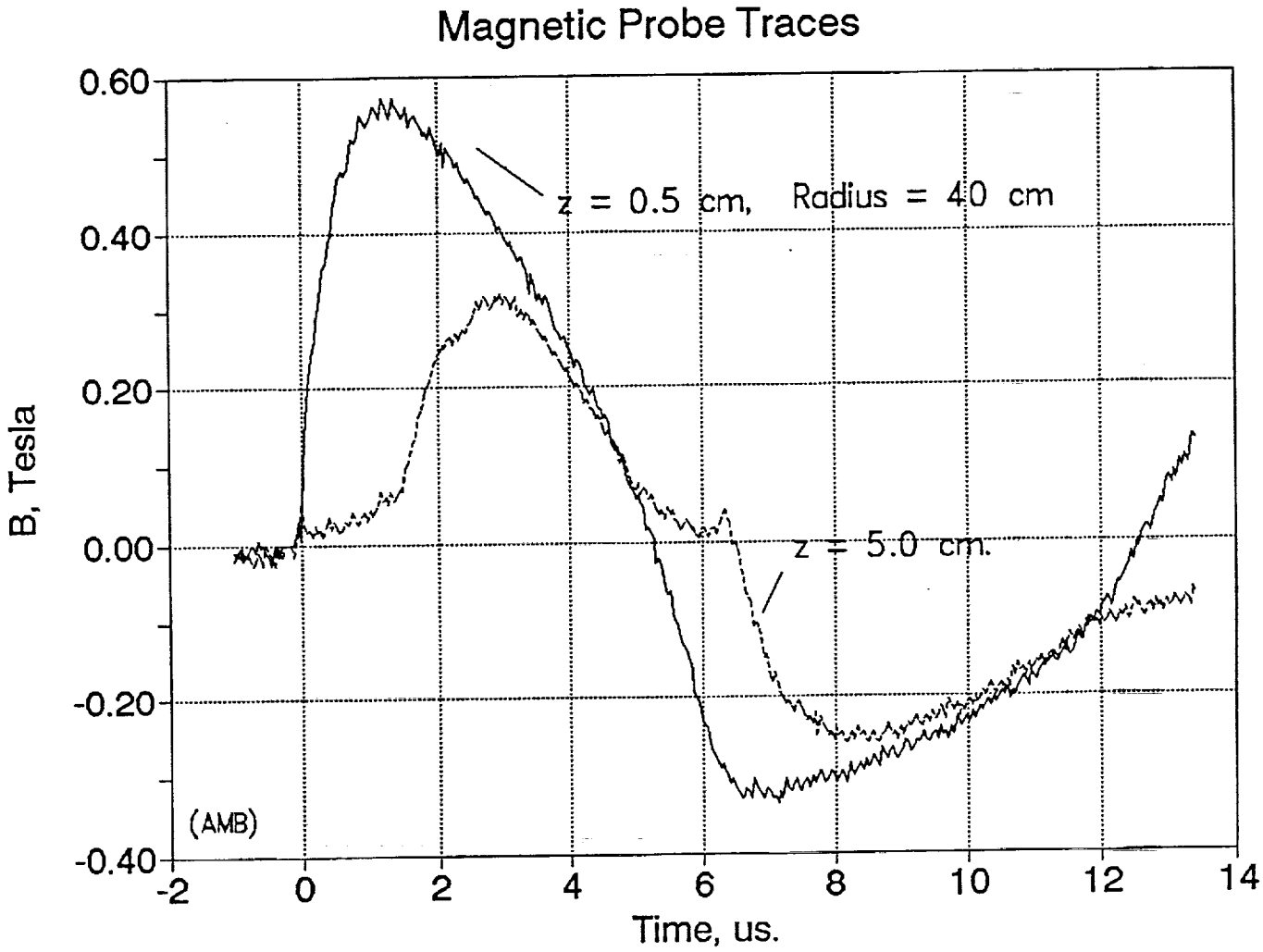
Magnetic Probe Traces
0.60
0.40
0.20
0.00
-0.20
-0.40
B, Tesla
z = 0.5 cm, Radius = 40 cm
z = 5.0 cm.
(AMB)
-2
0
2
4
6
8
10
12
14
Time, us.

Fig. 16

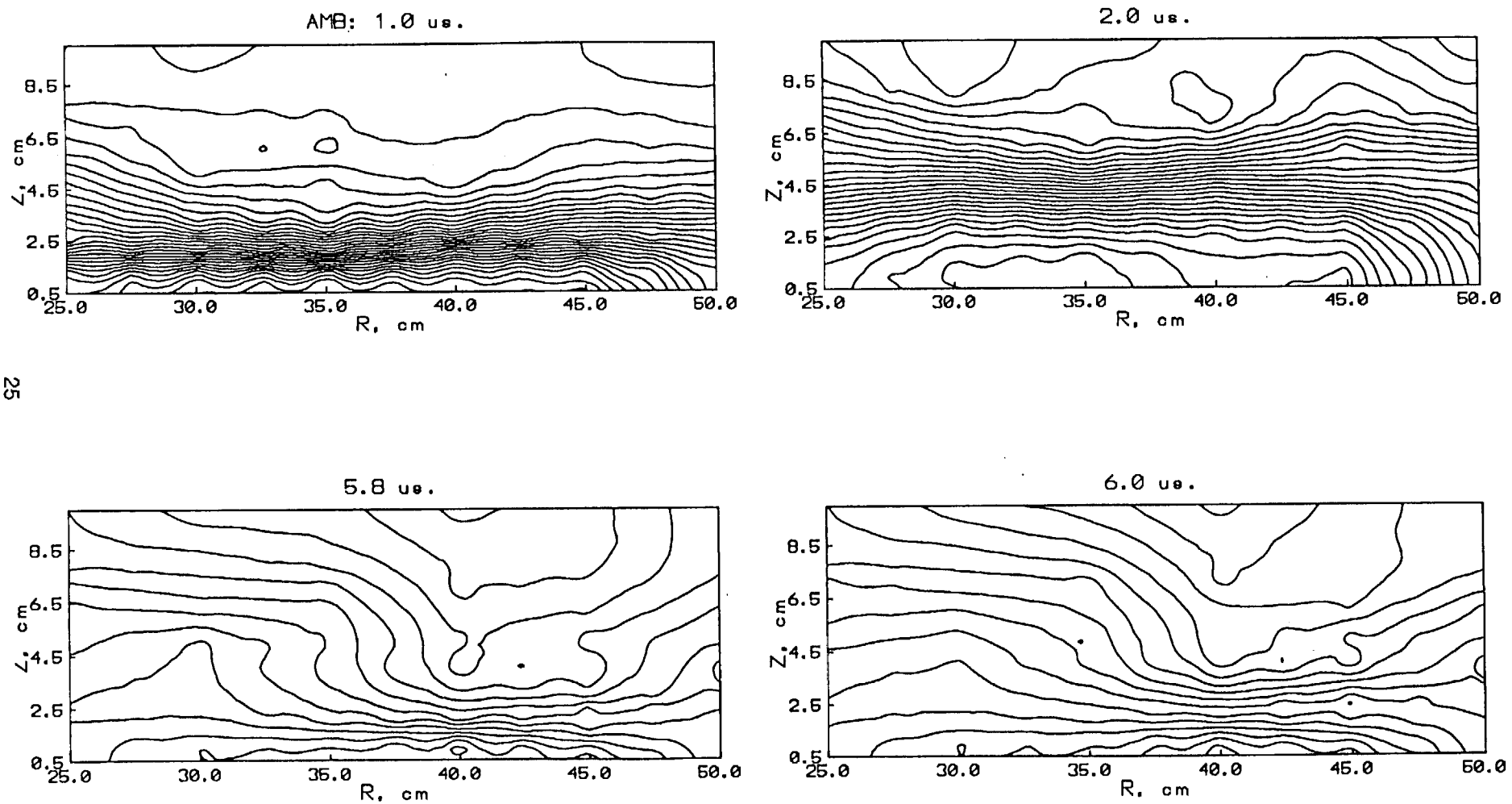

Figure 17. Magnetic Field Strength Contour Maps for 14 kV, 2.4 mg

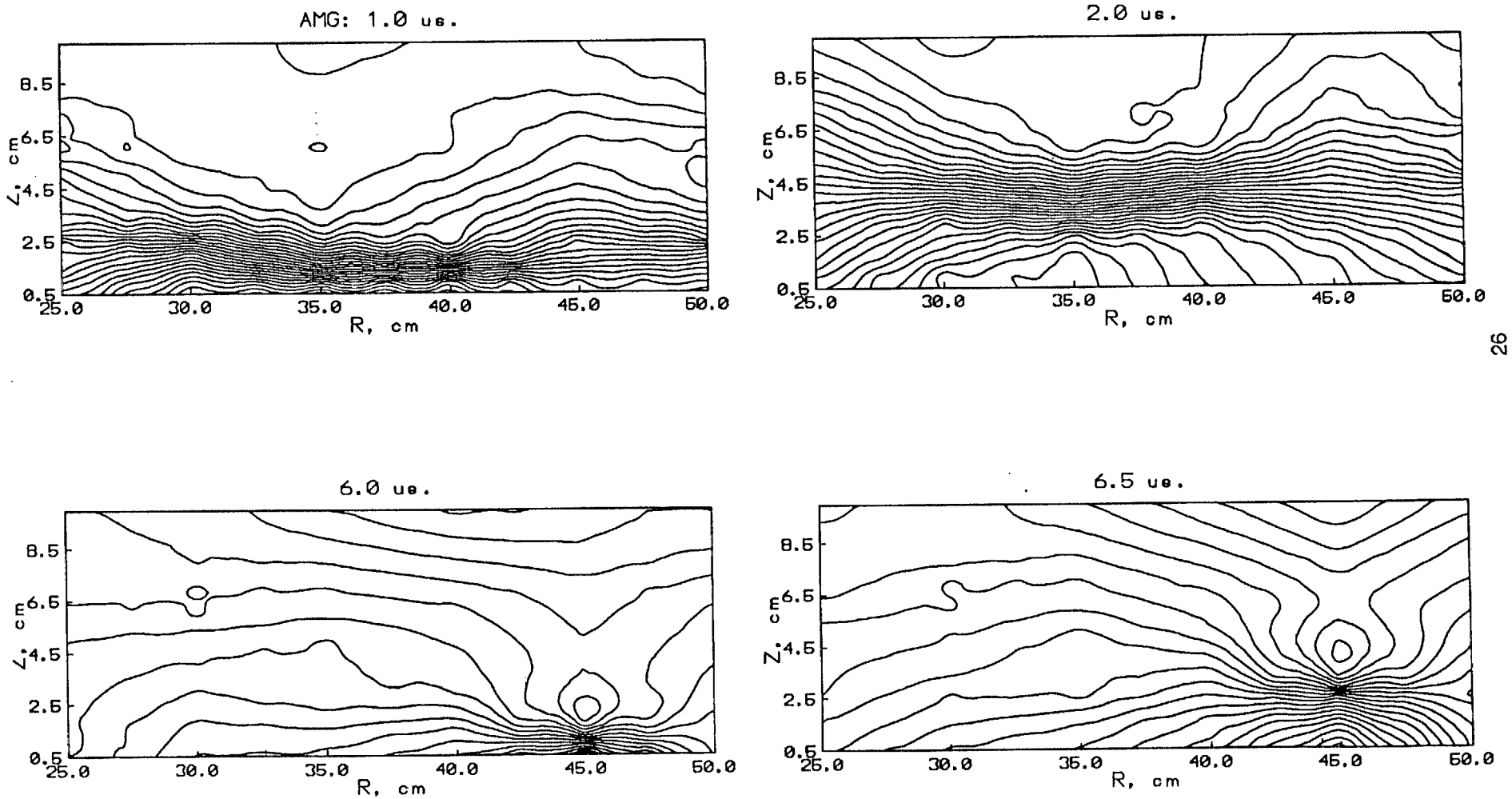

Figure 18. Magnetic Field Strength Contour Maps for 12 kV, 1.0 mg

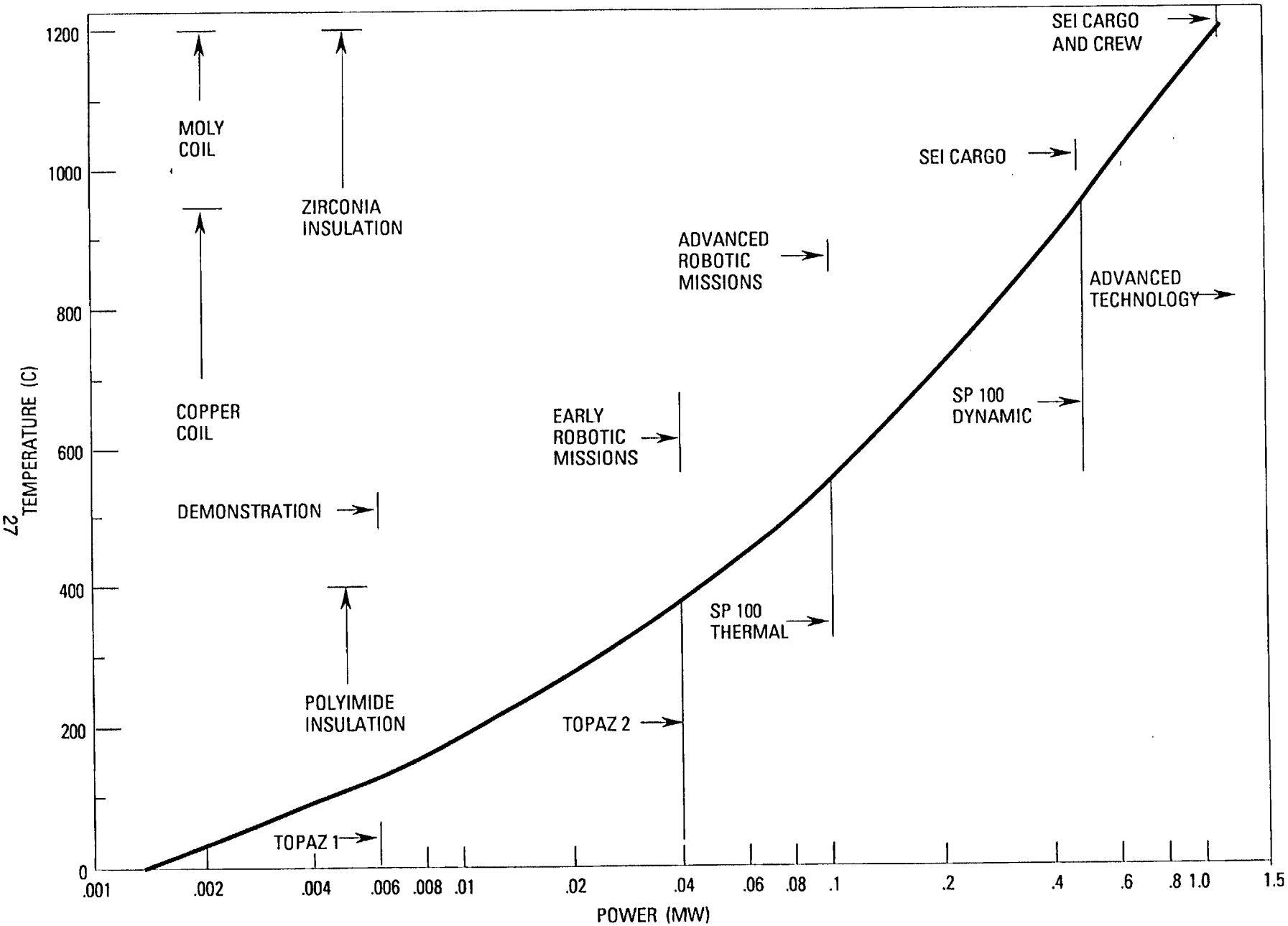

Figure 19. Power Source, Missions, Coil Temperature and Materials for a Wide Range of Power Levels

R9M 92.232.004a

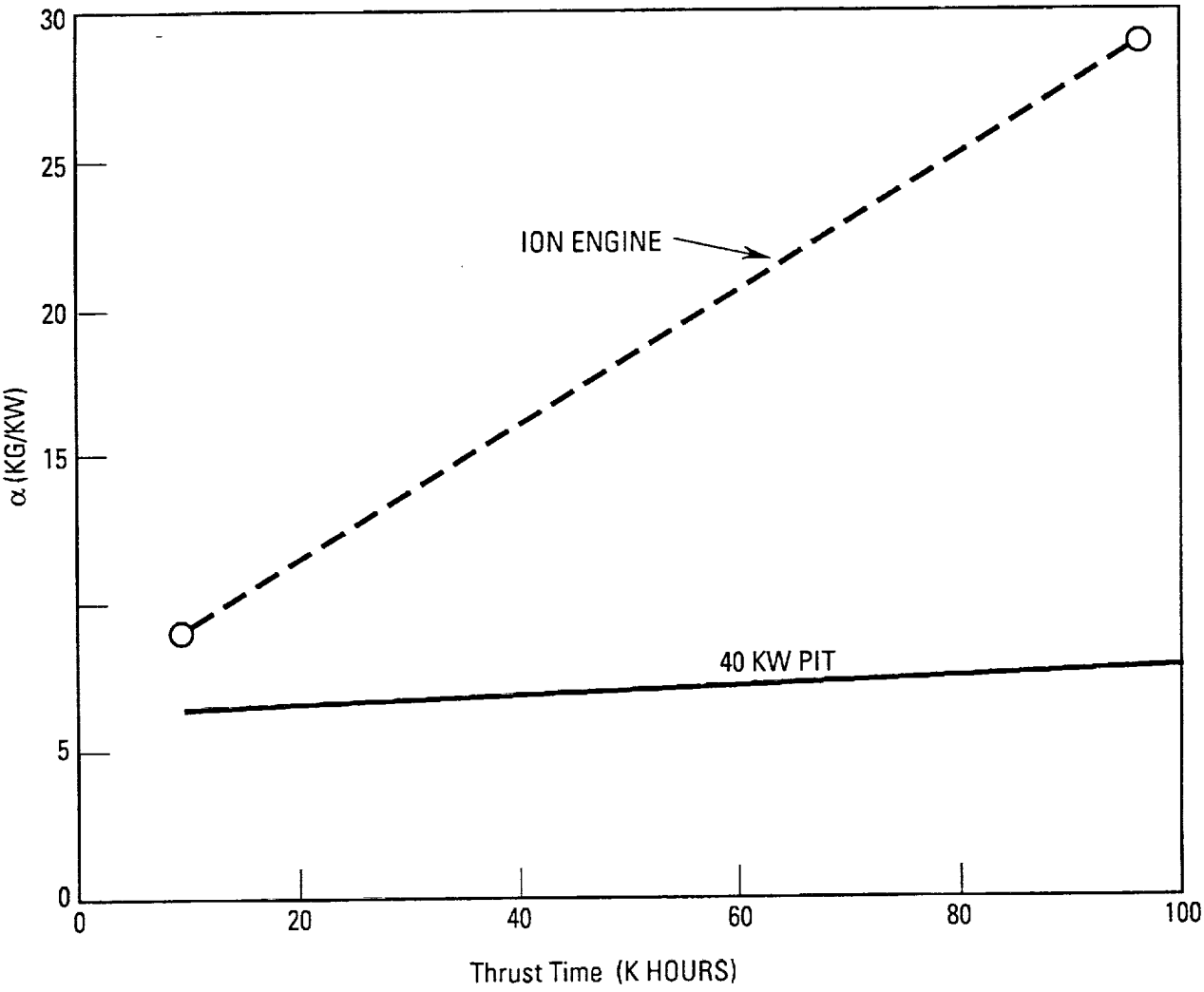

Figure 20. Effect of Thrust Time on PIT and Ion Engine Specific Mass

R9M 92.232.003a

Appendix A: PIT MkV Control System

1. Introduction

The design of the system developed for control of the pulsed inductive thruster PIT MkV has as its major assumption that all steps in preparation of the thruster for firing, the firing sequence itself, and the acquisition and logging of all data from a shot should be done from a central computer (PC). Diagnostic data other than the primary performance parameters (impulse, Mass increment, input energy), principally magnetic and electric probe data, are recorded on a fast digital transient analyzer and transferred to a second PC for archiving and subsequent analysis.

2. Hardware

As seen in Figure A-1, the computer is interfaced to the thruster system through two control modules, a Kiethley DAS-16G, and a Kiethley PIO-12. The former contains 16 A/D channels, four of which are used to input the following analog data:

- Main bank voltage. This signal is used to terminate bank charging at a preset voltage.
- Gas valve pulse capacitor voltage. Same charge function.
- Δp, the gas plenum pressure drop; this signal is a direct indicator of the propellant mass increment consumed during the shot.
- Thrust balance displacement. This damped oscillating signal indicates impulse delivered by the thruster.

In addition, the DAS 16G outputs digital signals that command firing of the pulsed gas valve and, after a suitable delay, the main capacitor bank.

The PIO-12 interface serves principally as a driver for solid state relays that perform AC switching functions, These are:

- Main bank charging.
- Gas valve capacitor charging
- Solenoid valve for spark gap flushing prior to shot.
- Solenoid for insertion of Δp manometer before shot.

3. Software

3.1 Main Menu

The operating program PITCON.EXE that is run upon bootup of the PC presents the operator with an initial menu of three items:

1. Set or revise calibration constants
2. Review logged data
3. Run the thruster

3.2 Calibration Menu

The first item displays and prompts for changes in:

- Thrust balance calibration, in Newton-seconds per unit amplitude from the transducer A/D converter.
- Mass increment in kG/unit from the manometer A/D
- Bank capacitance. Changes may occur due to replacement of individual capacitors in the bank.
- Propellant species.
- Name of file currently logging shot data.
- Number of records currently stored in log file. This enables the operator to resume a previous data sequence with a correct shot number.

3.3 Data Review Menu

The second main menu item allows examination of data logged from previous shots. These eleven data items are:

1. Date
2. Time
3. Propellant species
4. Main bank voltage
5. Valve capacitor voltage
6. Delay between valve and bank firings
7. Mass increment (Δm)
8. Impulse (I)
9. Efficiency (η)
10. Specific impulse (I_{sp})
11. Narrative remarks

All eleven items are displayed for any shot called by number from the data file currently opened by the program. Other data files can be examined after having been named in the calibration menu (above).

3.4 Run Menu

The third main menu option is for running the thruster. It opens a three-section screen, the first of which

- Provides for operation, from the keyboard, of each of the switching functions associated with the thruster, including separate manual firing of the valve or main bank, as may be required during testing.

- Prompts the operator to input the desired bank voltages and the delay between gas valve and main bank firing.

- Provides an automatic sequence of operations, leading to firing of the thruster:

  1. Spark gaps are flushed for five seconds.

  2. Gas valve capacitor is charged.

  3. Main bank is charged

  4. Electronic manometer is inserted.

  5. Gas valve is pulsed.

  6. After runout of the preset delay, spark gaps are fired.

Provision is made for automatic system shutdown if either of the two bank voltage signals fails to rise monotonically prior to reaching its preset voltage. The operator may also "scram" the system at any time by pressing "Z" on the keyboard.

Immediately subsequent to the shot, a data acquisition, processing, and display sequence is initiated:

- Displacement of the thrust balance, oscillating from the impulse delivered by the thruster, is sampled approximately 10^3 times per second. Four successive extrema are identified and recorded; these are extrapolated exponentially back to zero time to obtain a true amplitude. Multiplication by the calibration constant then yields an impulse figure (I) to the logging routine.

- After a delay of approximately ten seconds which allows restoration of pressure equilibrium in the thruster gas supply lines, the differential pressure transducer (manometer) is read, and its calibration constant multiplied into the reading to give Δm.

- Voltages of the main and valve banks at the time of firing are recorded.

- Finally, I, Δm, C (main bank capacitance), and the charge voltage V are combined to give the specific impulse (I_{sp}) and the thrust efficiency (η). These quantities are displayed on the second section of the operating menu screen.

The third section (bottom) of the operating menu screen offers the operator the option of saving the operating parameters, transducer readouts, and computed performance data of the shot to the disk archive. A "Y" then elicits a prompt for input of narrative remarks of up to two lines; upon receipt of these, the program records the twelve items mentioned earlier to the active hard-disk data file.

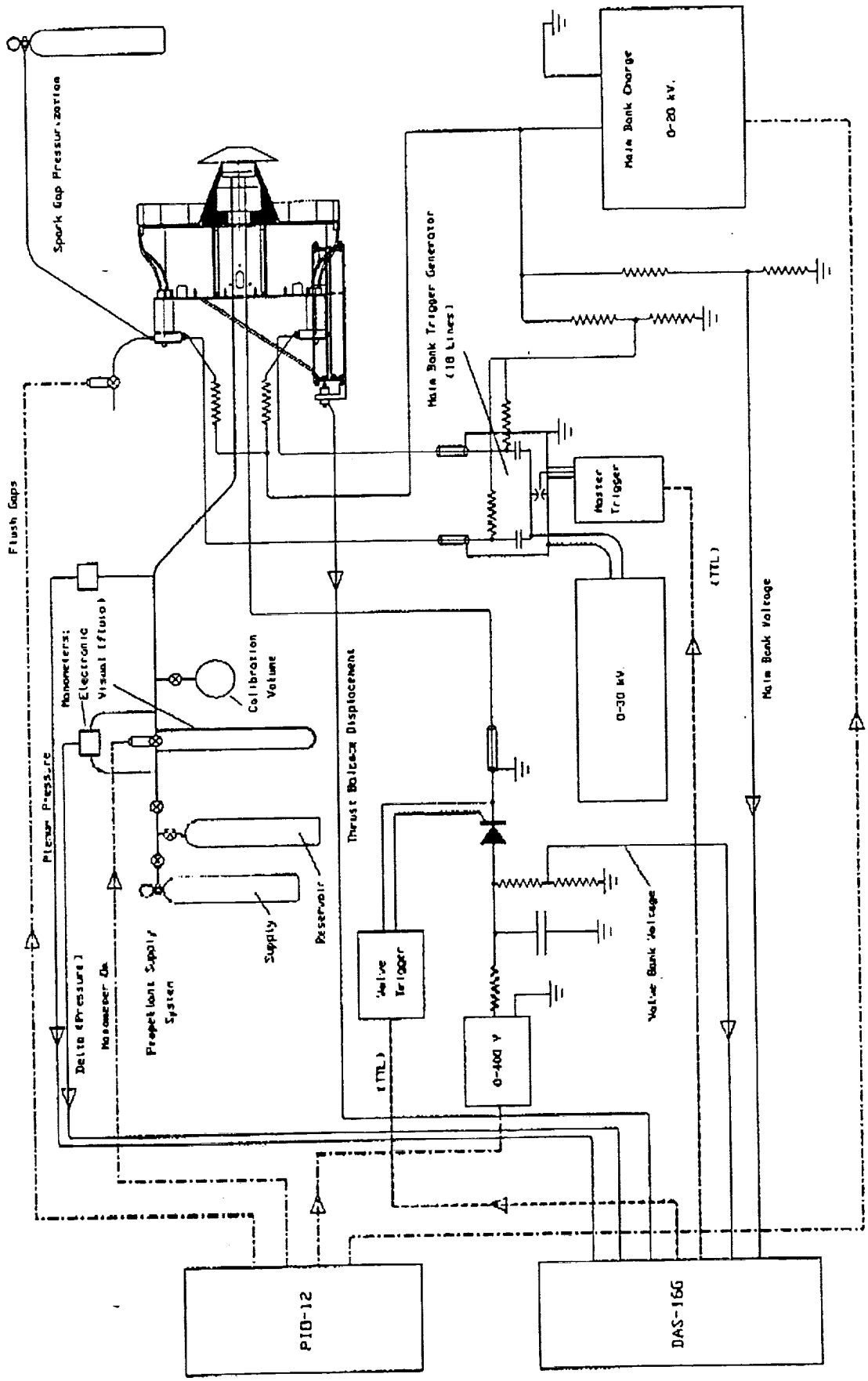

PIT MkV System Organization

Fig.A-1

Appendix B: Thrust Balance Calibration

1. Procedure

Calibration impulse is delivered to the thruster by a simple pendulum consisting of a ball of clay suspended by a thin string. The pendulum is attached to the vacuum tank wall directly above the forward extremity of the gas valve assembly, to which a flat plate is mounted. After release from a horizontal position, the ball strikes the plate, and comes to rest without rebound. Thus, the impulse to the thruster is given by

$$\Delta I = m\sqrt{2gh} \ ,$$

where m is the mass of the ball, and h the vertical distance between its release and impact points. We measure both parameters to an accuracy of approximately 0.3%; thus, we know the impulse to the same order.

2. Noise and Data Scatter

In order to provide significant response to an impulse less than 0.1 N-s when the oscillating mass is 200 kg, the restoring spring constant of the thrust balance is made extremely small, to the extent that its response to the ambient seismic background is significant. When operated at a Q of about 20, the balance executes an approximately sinusoidal oscillation at a frequency of 1 hz with an amplitude corresponding to .003-.005 N-s. This noise is added to the calibration impulse, resulting in data scatter.

Suppose that the thruster is oscillating at amplitude x_o, frequency ω, and phase ϕ_o, when it receives a velocity increment v_1 from the calibrator. The resultant amplitude x can be shown to be

$$x = \sqrt{x_o^2 + \frac{2x_o v_1}{\omega}\cos\phi_o + \frac{v_1^2}{\omega^2}}$$

$$= x_o + \frac{v_1}{\omega} \qquad \text{for } \phi_o = 0$$

$$= x_o - \frac{v_1}{\omega} \qquad \text{for } \phi_o = \pi$$

A distribution of N measurements made at random phases ϕ would be strictly bounded by the $\phi = 0$ and $\phi = \pi$ limits. Between them it may be seen that the distribution will be peaked near the limits, because in its sinusoidal motion, the oscillator is most often found near its low velocity points. The actual distribution function is

$$f(x) = \frac{1}{\pi\sqrt{x_o^2 - x^2}}$$

While one may assign as the nominal response of the balance the mean of the N readings, a more complicated problem is the assignment of confidence limits for the mean. For a normally distributed variable, the problem is simply that of calculating the standard deviation of the data set. Applied to these data, this approach produces anomalous results; for example, the standard deviation points of a 15-sample set were found to be outside the absolute bounds of the set.

Rather than attempting an analytical solution of this problem, we have approached it numerically. Values of amplitude x were obtained by taking N samples of a constant impulse contaminated by a random-phase sinusoidal noise; these data were averaged, and the process repeated 100 times, to obtain 100 means. These means are themselves normally distributed, so that their standard deviation may be taken as the 68% confidence limit for a single mean.

The calibration run that has been used for all of the MkVa data applied an impulse of 0.111 N-s for each of 14 samples. Outputs had digital values from 698 to 734 with a mean of 715.4. Accordingly, we have done the simulation with an assumed true impulse of 720 units mixed with a noise amplitude of 20 units, and N=14. The standard deviation of 100 means is typically about 7 units, or 1% of the mean. For comparison, the standard deviation of the single data set, using the formula appropriate to a normal distribution, is 20 units.

Figure B-1 is the distribution of means for a typical simulation, while Figure B-2 is the distribution of amplitudes for the entire 1400 individual data points; it clearly follows the theoretical f (x) given above.

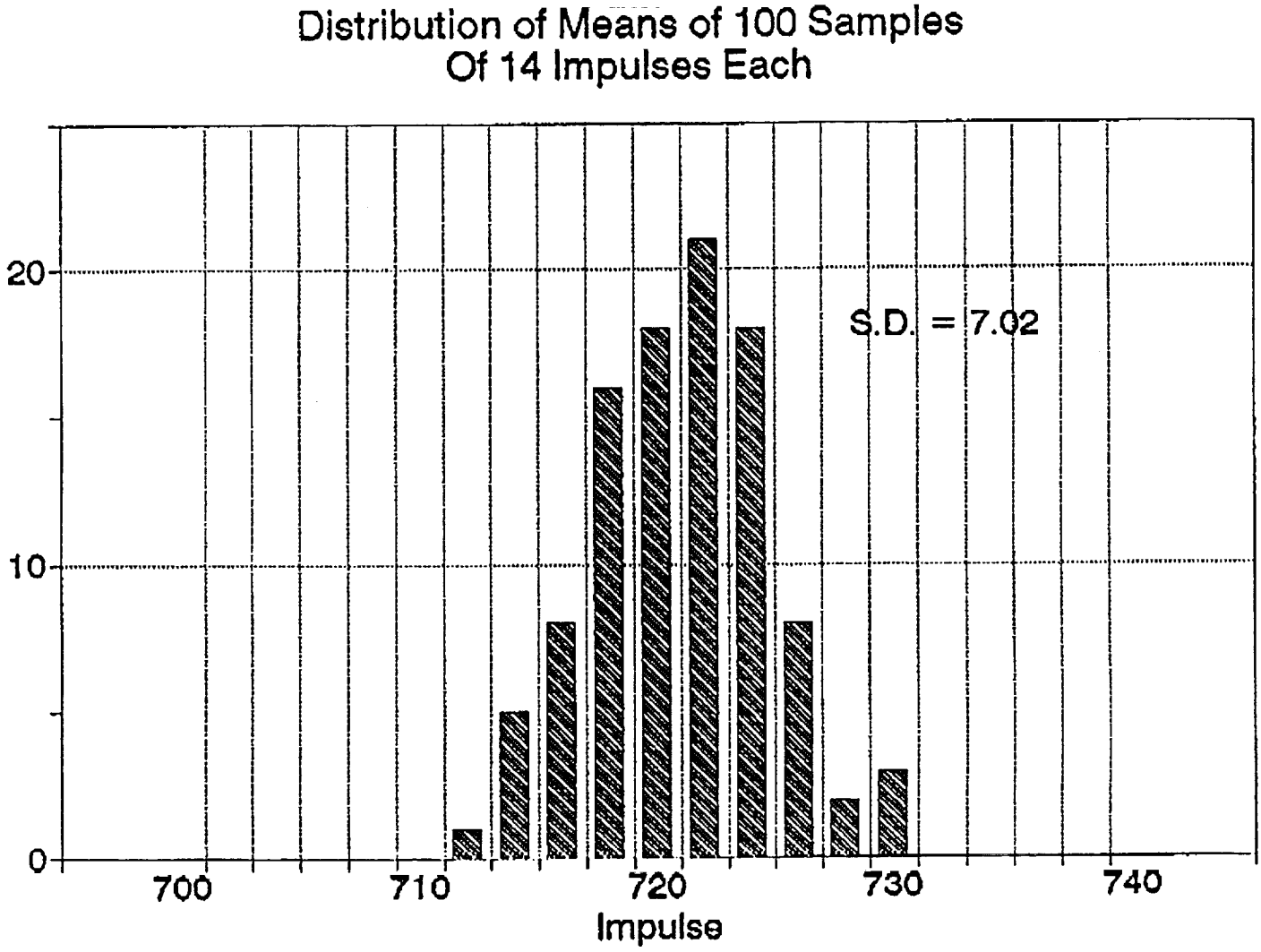
Distribution of Means of 100 Samples
Of 14 Impulses Each
S.D. = 7.02
20
10
0
700
710
720
730
740
Impulse

Fig.B-1

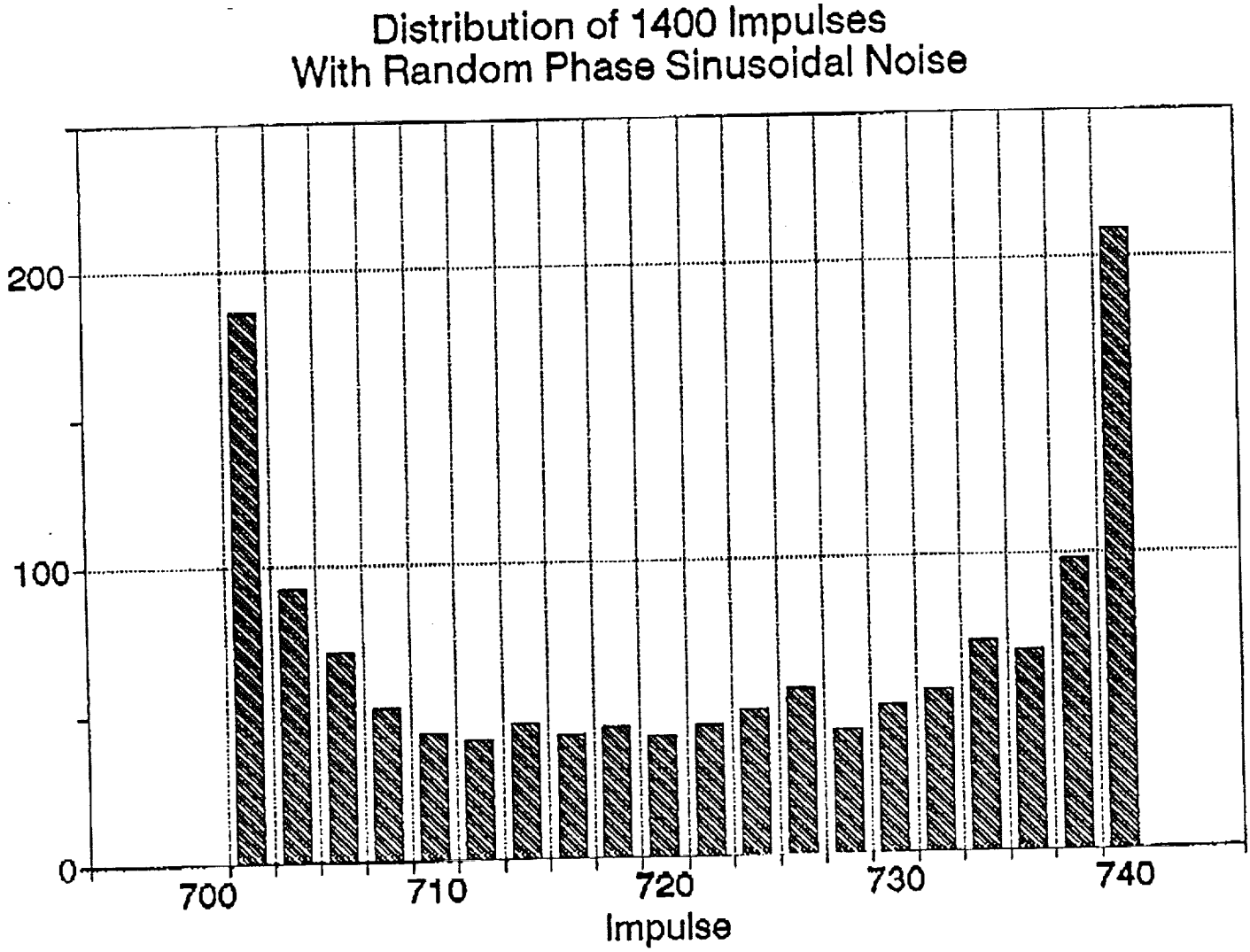
Distribution of 1400 Impulses
With Random Phase Sinusoidal Noise
200
100
0
700
710
720
730
740
Impulse

Fig.B-2

Appendix C: PITV: Simulation of Pulsed Inductive Thruster

1. Introduction

This appendix describes a simulation code written to serve as a design aid for the pulsed inductive thruster. It incorporates a fairly accurate representation of the electrical circuit, and a more approximate representation of the accelerated plasma; nevertheless, it yields reasonably close predictions of thruster performance.

---Appendix Nomenclature---

English

a,b:	Coil inner and outer radii respectively	(m)	R_p:	Resistance of plasma current loop	(Ω)
A:	Annular coil area	(m^2)	R_e:	External circuit resistance	(Ω)
C:	Equivalent circuit capacitance	(F)	t:	Time	(s)
F_i:	General system force along x_i	(N)	V:	Voltage on equivalent circuit capacitance	(V)
Fz:	Axial plasma force per unit area at position z	(N/m^2)	v(Z):	Plasma velocity at axial position z	(m/s)
F'z:	Axial force on plasma	(N)	x_i:	General system coordinate	(m)
I_1:	Circuit current	(A)	z_o:	Decoupling stroke length	(m)
I_2:	Plasma current	(A)	z:	Axial position of plasma current sheet	(m)
L_o:	Unloaded coil inductance	(H)	z^1:	Dummy index of integration	(m)
L_e:	Parasitic inductance	(H)			
L(Z):	Circuit inductance for current sheet at z	(H)		Greek	
M:	Mutual inductance	(H)	δ_a:	Current sheet thickness at time t	(m)
m(z):	Mass per unit area entrained at z	(kg/m^2)	δ_s:	Current sheet thickness at t = o	(m)
Q:	Charge in equivalent circuit capacitance C	(C)	δ_m:	Final current sheet thickness	(m)
q:	(Energy stored)/Energy dissipated) per cycle		η:	Plasma resistivity	(Ω-m)
			μ_o:	Permeability of space	(H/m)
			ρ(Z)	Axial distribution of plasma mass per unit area at t=0	(kg/m2)

---

2. System model

2.1 Electrical circuit

The Pulsed Inductive Thruster (PIT) consists of a capacitive energy storage bank that is discharged into the primary winding of a transformer whose secondary is an annular ring of plasma. Inasmuch as the force between the two circuits is repulsive, they move apart, with the result that the mutual inductance (and coupling coefficient) of the circuits decreases monotonically. The presence of time-varying inductance in the system complicates its analysis, because such terms are dimensionally resistances, and accordingly, consume energy when multiplied by current squared. The primary circuit external to the coil has some inductance, usually dubbed *parasitic* because it is detrimental to efficiency, and the entire circuit possesses a finite resistance as well. Good engineering design will keep it small, so that it consumes a negligible fraction of thruster input energy.

The secondary is a simple annular ring, so one cannot define a separate parasitic inductance component for it; however, its resistance is usually large enough to be a major determinant of thrust efficiency.

The thruster circuit and its equivalent circuit, which will be used in deriving the system equations, are shown in Figure C-1.

2.2 Thruster Geometry

The primary coil is a flat spiral annulus having outer radius *b* and inner radius *a*, and one turn. The plasma secondary has the same radial dimensions and a thickness δ_a. As it separates from the primary coil to distance z, the mutual inductance is an exponentially decreasing function of z; its dependence will be detailed in Section 3.

2.3 Plasma Model

Three parameters are assumed to characterize the plasma:

- Initial density distribution of the propellant at time of firing. Several analytic distributions have been used (e.g., Gaussian, exponential), but the current one is a simple linear drop as a function of z from a maximum at the coil surface, to zero at $z = \delta_m$, which is the closest approximation to the distribution actually measured with the fast ionization gauge probe. It is assumed that the gas is fully ionized at the start.

- Plasma resistivity, η. It is known from earlier work on medium-weight plasmas in pulsed systems that electron temperature tends to be "thermostatted" to a fairly narrow range over a wide range of current density or plasma density, so that the assumption of a uniform and constant resistivity is fairly good. As an example, the temperature of electrons in a pulsed Argon plasma is usually near 3 ev, and the resistivity near 5×10^{-5} ohm-m.

- Initial current-sheet thickness (δ_s). During the breakdown and ionization of a real plasma, resistivity swings from a high initial value to the nearly steady value characteristic of the rest of the acceleration. The flow of current at early times is therefore in a layer thicker than would result from classical diffusion at constant resistivity. This dimension is assigned as a starting parameter of the calculation; its value is chosen by reference to previous experimental probe measurements. Subsequent to the start of the calculation, the layer is assumed to thicken by classical diffusion ($\delta_a(t)$).

3. Equations

3.1 Electrical

In the equivalent network of Figure C-1, C is the bank capacitance, R_e the primary circuit resistance, L_o the unloaded coil inductance, and L_e parasitic inductance, M is the mutual inductance, a function of z and hence, of time, and R_p is the resistance of the plasma loop. The two mesh equations are

$$-M\frac{dI_1}{dt} + L_o\frac{dI_2}{dt} - I_1\frac{dM}{dt} + I_2R_p = 0 \qquad \text{(C-1)}$$

$$(L_o + L_e)\frac{dI_1}{dt} - M\frac{dI_2}{dt} + I_1R_e - I_2\frac{dM}{dt} = \frac{Q}{C} \qquad \text{(C-2)}$$

These may be rearranged to give derivatives of the two currents:

$$\frac{dI_1}{dt} = \left(\frac{L_o Q}{C} - L_o R_e I_1 - M R_p I_2 + (L_o I_2 + M I_1)\frac{dM}{dt}\right) / \left(L_o (L_o + L_e) - M^2\right) \quad \text{(C-3)}$$

$$\frac{dI_2}{dt} = \left(M \frac{dI_1}{dt} + I_1 \frac{dM}{dt} - R_p I_2 \right) / L_o \quad \text{(C-4)}$$

$$\frac{dQ}{dt} = - I_1 \quad \text{(C-5)}$$

The dependence of M and dM/dt upon plasma position and velocity has been obtained from an experimentally measured dependence of the total circuit inductance (as seen from the primary terminals) as a function of z. An aluminum plate annulus, having the outer and inner radii of the coil, was placed over the coil at various separations, and the circuit inductance measured at each position by a magnetic probe measurement of the field oscillation frequency and decrement when the capacitor bank, charged to 5 kV, was switched into it.

The total inductance L (z) was found to be very closely approximated by the simple exponential function

$$L(z) = L_e + L_o (1 - \exp(-z/z_o)), \quad \text{(C-6)}$$

where

L_o = 660 nH (Unloaded coil inductance)
L_e = 80 nH (Parasitic inductance)
Z_o = 7.5 cm (Decoupling length)

Figure C-2 displays the experimental measurements of L(z), as well as curve for Equation (C-6).

The decrement of the circuit oscillation for the unloaded ($z = \infty$) case corresponds to a Q of 80, which implies a total circuit resistance R_e of 5 mΩ.

A result easily derived from Figure C-1 is that at the coil terminals (i.e., excluding the parasitic inductance and resistance), the measured circuit inductance will be

$$L = L_o - \frac{M^2}{L_o} \quad \text{(C-7)}$$

Combining with Equation (C-6) above, one obtains

$$M = L_o \exp(-z/2z_o), \quad \text{(C-8)}$$

$$\frac{dM}{dt} = - \frac{L_o}{2z_o} \exp(-z/2z_o) \frac{dz}{dt}, \quad \text{(C-9)}$$

Plasma resistance R_p is related to resistivity and geometrical parameters by

$$R_p \simeq \frac{\pi (b + a) \eta}{\delta_a (b - a)} \quad \text{(C-10)}$$

The current sheet thickness δ_a (t) begins at a value of δ_s and thickens by diffusion, so that the plasma loop resistance decreases with time. We simulate this process by first defining a time t_o which is that time that would be required for an original delta-function current distribution to diffuse to δ_a:

$$t_o = \frac{\mu_o \delta_s^2}{\eta}, \tag{C-11}$$

Then, the diffusion proceeds onward from this equivalent time when the acceleration begins:

$$\delta_a (t) = \sqrt{\frac{\eta}{\mu_o}(t+t_o)} \tag{C-12}$$

A number of energy losses that might be separately treated in a more detailed simulation are here subsumed into the plasma resistance, since plasma resistive heating is what supplies the thermal energy for radiation, ionization, dissociation, and temperature increase of plasma electrons. Subsequent to the early ionization and dissociation of the propellant, it can be assumed that plasma assumes a nearly constant temperature, so that resistive power is balanced by radiation,[1]

3.2 Equation of Motion

A general theorem states that if the inductance of a circuit depends explicitly upon some spatial coordinate x_i, then when current I is passed through the inductor, a force is exerted along x_i equal to

$$F_i = \frac{I^2}{2}\frac{\partial L}{\partial x_i}, \tag{C-13}$$

Thus, from Equation C-6, we immediately derive

$$F_z = \frac{L_o I^2}{2 z_o} \exp(-z/z_o), \tag{C-14}$$

For a current sheet moving through a mass density distribution p(z) and entraining the mass it encounters in the "snowplow" approximation, the force per unit area is given by

$$F_z' = m(z)\frac{dv_z}{dt} + \rho(z) v_z^2, \tag{C-15}$$

where $$m(z) = \int_{z=o}^{2} \rho(z')\, dz'. \tag{C-16}$$

[1] In one version of this simulation, the plasma was given a fixed high resistivity for enough time to complete first ionization of each propellant molecule, after it was returned to the value assigned in the initial menu. The efficiency difference between this and a consistant resistivity model was not usually greater than about 1% for the range of parameters covered by the PIT MkVa experiments.

Work going into the first term goes entirely into increasing the directed (center-of-mass) kinetic energy of the plasma, whereas work done by the second term is split equally between internal heat of the plasma and directed energy. It is therefore desirable from the standpoint of propulsive efficiency to minimize the integrated contribution of the second term by keeping the initial plasma distribution within a value of z much smaller than the effective acceleration stroke length, i.e., to keep $\delta_m << z_o$.

The equations of motion of the plasma may now be written

$$\frac{dv_z}{dt} = \left(\frac{L_o I_1^2}{2 z_o A} \exp(-z/z_o) - \rho(z) v_z^2 \right) / m(z) \qquad \text{(C-17)}$$

$$\frac{dz}{dt} = v_z , \qquad \text{(C-18)}$$

where $A = \pi (b^2 - a^{2)}$ is the area of the coil.

4. Integration

Equations (C-3),(C- 4), (C-5), (C-17), and (C-18) are integrated with a standard ODE solver (LSODE). The PITV program prompts input of propellant mass (m_o), propellant depth (δ_m), capacitance, resistivity (η), initial current sheet thickness (δ_e), and bank voltage. L_e, L_o, z_o and R_e are set at the measured values given earlier.

Time, bank current (I_1), v_z, and z are printed out for each 100 nanoseconds of discharge time, both to the screen and to a data file. After 12 microseconds, the run is terminated, and efficiency, I_{sp}, and total impulse are displayed.

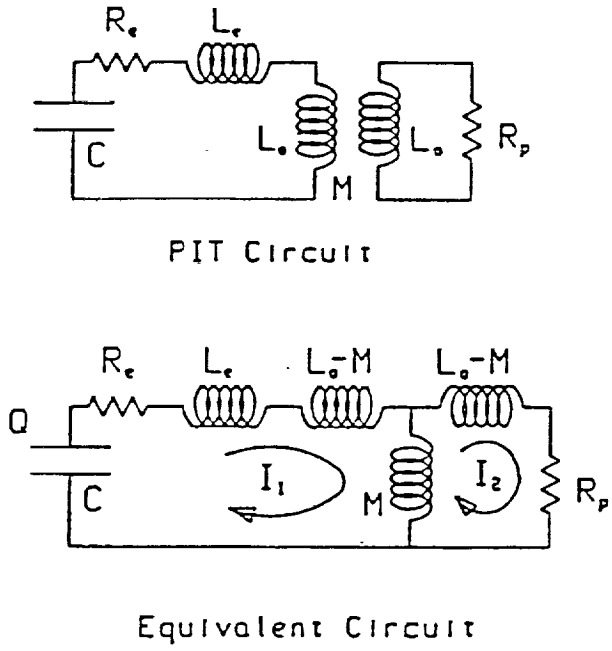

Figure C-1 Electric Circuit for PIT and its Equivalent Circuit.

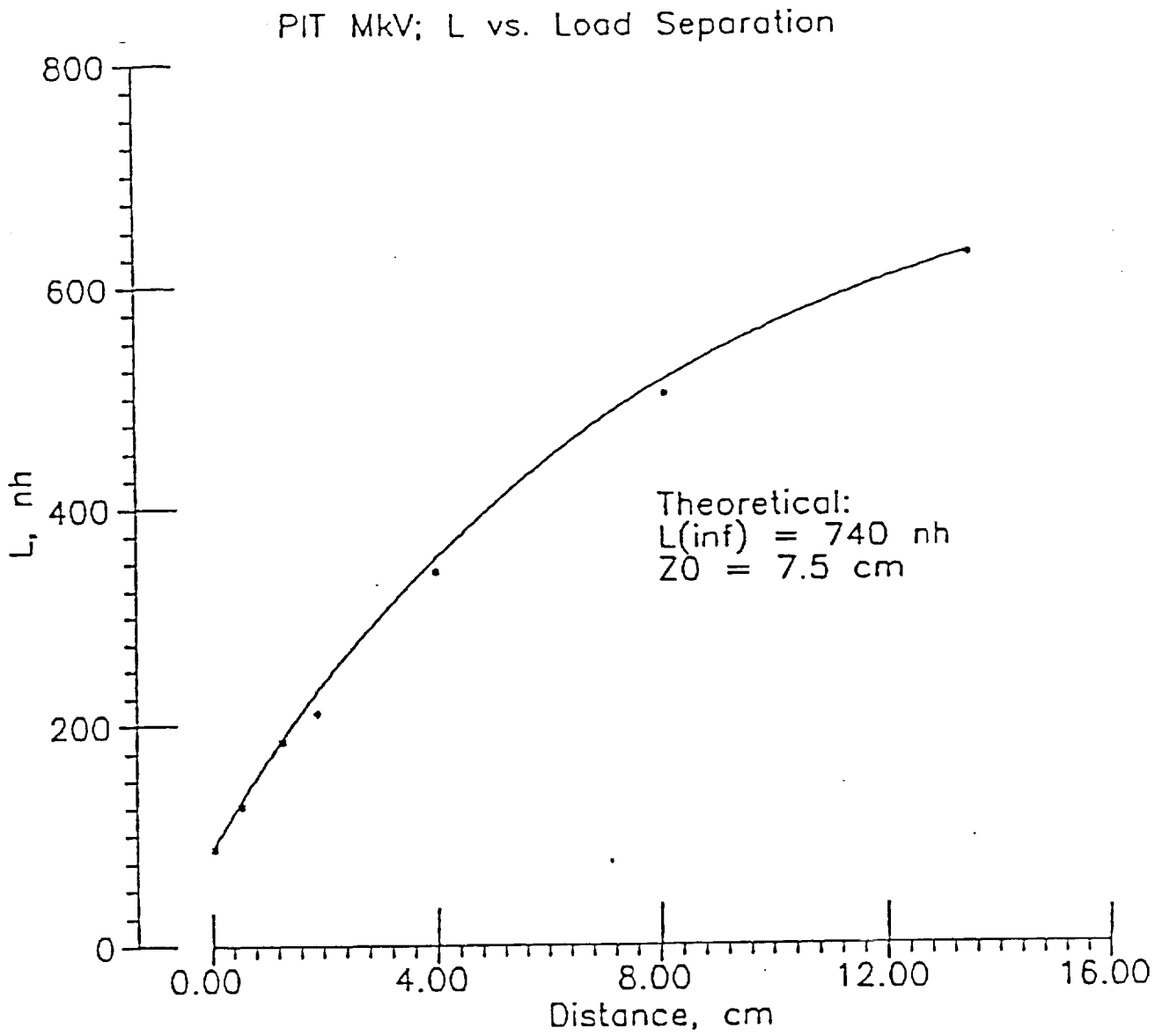

Figure C–2 PIT MkV; L vs. Load Separation

Appendix D: Facility Effects

1. Introduction

The vacuum facility in which these experiments have been performed is non-ideal in two important respects. First, the base vacuum with the thruster in place is 0.2 micron. While this background is not a significant addition to the density of the injected propellant, it increases the possibility that enough gas could adsorb on the coil insulator surface to provide an important mass addition when the discharge dislodges it.

The second problem is that only about one cubic meter of tank volume lies in front of the thruster. There is a possibility that the plasma, whose directed kinetic energy alone is in excess of 2 kilojoules, will desorb a significant pulse of gas from the wall it encounters, and that this gas will apply a pressure transient to the coil face, thus corrupting the impulse reading. In normal startup of the thruster after a pump down of the vacuum system, this effect is very apparent (although it does not appear upon startup after a long quiescent period in the vacuum). Initial impulses may indicate efficiency over 70%; however, after a few tens of shots, the readings decay to a lower asymptotic value.

It remains possible that the impulse obtained during steady running still contains a component of a tank pressure transient that reproduces well from shot to shot, or that a reproducible desorbed mass increment from the coil surface accompanies the plasma from each discharge. We argue here that the presence of these components will leave a particular signature on the impulse data and η-I_{sp} curves that does not appear in our present results.

2. Δm Effects

To illustrate, we use the 16 kV ammonia data, where, because of the high energy of the plasma, facility effects should be strongest. Figure D-1 gives the totality of the raw impulse data (I) for this run, plotted against injected mass. It is shown that these points can be fitted well with a simple parabolic curve whose origin coincides with the I vs. mass origin.

A more useful presentation of impulse data is that of I^2 vs. injected mass, given in Figure D-2. Here, a straight line through the origin has been fitted to the experimental points. The slope of this line is proportional to efficiency. Since.

$$\eta = \frac{mv^2}{CV^2}$$
$$= \frac{1}{CV^2}\frac{I^2}{m},$$

it can be seen that dividing the slope by twice the bank energy yields efficiency, which in this instance, is 51.8%. Of more importance here, however, is the statistical confidence that the data project to a value of zero impulse for zero injected mass. Were there extra mass in the plasma from coil surface desorption, one would expect a leftward shift of the data points, as illustrated by the open circles that represent the addition of 0.3 mg. for each shot.

A regression analysis of the experimental points gives the value of spurious mass implied by the data set (i.e) the negative x-intercept of a linear regression line), together with a probable error. In this instance it is

$$\Delta m = 0.017 \pm 0.076 \text{ mg}$$

One may then conclude that there is no desorbed mass component greater than 0.1 mg in the 16 kV ammonia data.

3. ΔI Effects

In Figure D-3, a similar comparison, in an I^2 vs. mass plot, is made between the actual data and the same points shifted by the addition of an extra impulse of 0.01 N-s to each shot. Here, the difference between the original and the corrupted data varies as the square root of the mass; the dashed line is the new position of the original straight line. Identification of a data set as being distorted by constant extra impulse is difficult here, since the quadratic fitting curve comes very close to intersecting the origin; moreover, given the scatter of this data set, one could reasonably fit the offset points with a straight line through the origin, and conclude that thruster operation was normal, but at a higher efficiency than that of the original data. We cannot, therefore, use this data presentation format to decide the matter of spurious impulse.

Analysis of η–I_{sp} curves is more helpful. In Figure D-4, we plot three curves. The lower curve (open circles) is generated by the PITV simulation program, assuming an electron temperature that limits the best efficiency to slightly over 40%. I_{sp} is varied, as in our actual experiments, by varying the injected mass. As it should for the parameters of this thruster, efficiency flattens out at about 5000 s.

The second curve (asterisks) is generated by adding 0.3 mg to the injected mass at each point, and moving that point to the position one would calculate for it, observing the increased impulse, but being unaware of the increased mass.

The third curve (solid circles) results from the addition of 0.01 N-s impulse to what would have been the correct reading for each point in the absence of a tank effect.

One may now notice a qualitative difference between the distorted curves and the original; the upper curves have positive slopes where the correct η-I_{sp} characteristic should be level, and the difference between the slopes becomes greater at high I_{sp}, where the extra mass or impulse becomes a large fraction of the total.

The data that it is appropriate to examine for this effect are the 14, 15, and 16 kV runs in ammonia, because for each, the critical mass dropoff of efficiency (which would mask a rise due to ΔI) occurs above 5000 s I_{sp}. In each of these runs, the data reach a maximumn at about 5000 s, and decrease thereafter. There is no indication at all of a rise of the 14 or 15 kV data above the predicted performance curve.

The 16 kV data exhibit what might be a tank-generated impulse component. The mean efficiencies of the 0.69 mg and 1.05 mg points do not appear to drop as rapidly with increasing I_{sp} as does the simulation, and so, may lie on a curve of higher slope. The difference corresponds to an additional impulse of about 0.003 N-s. Given the small number of points and their large scatter, however, the identification of a spurious impulse from this data set is very tenuous.[1]

[1]The PITV simulation does not include impulse from thermal expansion of the accelerated plasma, since it should usually be a very small correction. A rough estimate of this impulse, based on the 0.67 mg, 10 ev plasma acting from 5 μsec against the thruster, gives a value of about 0.003 N-s, so that this, rather than a facility effect could explain the discrepancy between the simulation curve and the 16 kV data.

4. Conclusions

Analysis of the raw impulse data from the 16 kV run with ammonia propellant shows that these data are inconsistent with the hypothesis of a constant extra mass increment being added to that injected through the propellant valve.

Spurious impulse from tank ejecta, if present at all, is not large enough to have significantly affected measurements of thruster performance.

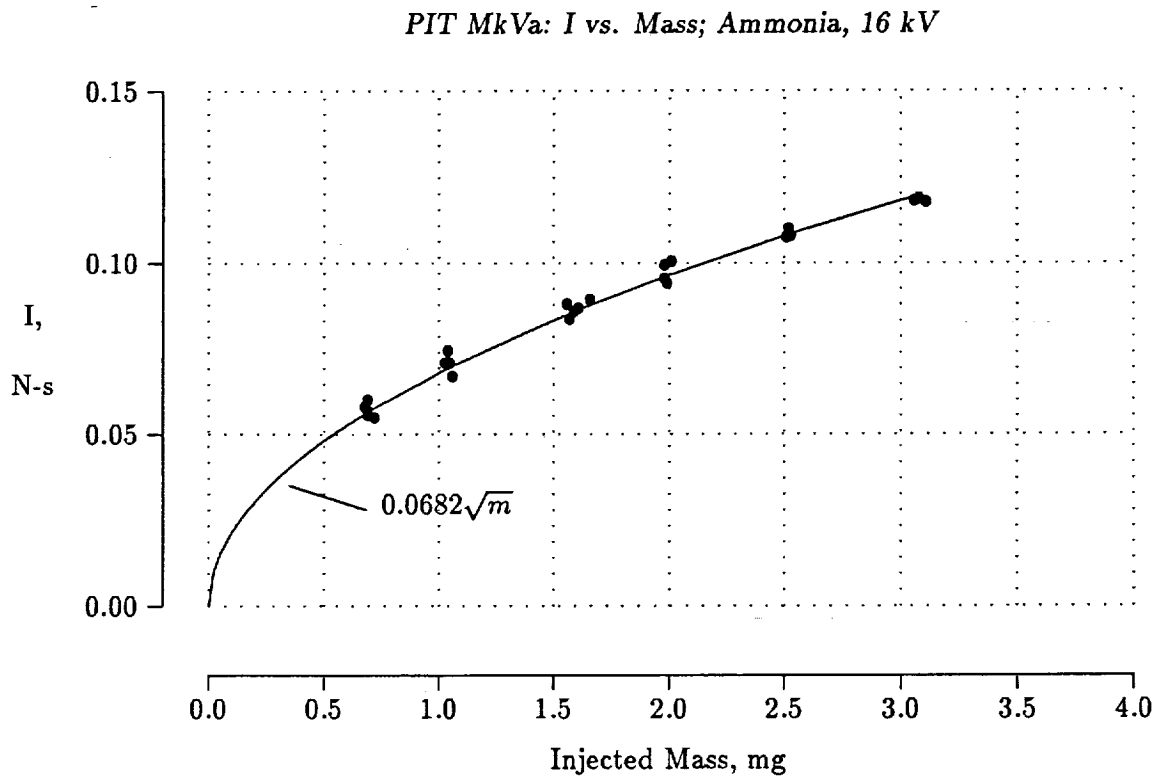
PIT MkVa: I vs. Mass; Ammonia, 16 kV
0.15
0.10
0.05
0.00
I,
N-s
$0.0682\sqrt{m}$
0.0
0.5
1.0
1.5
2.0
2.5
3.0
3.5
4.0
Injected Mass, mg

Fig.D-1

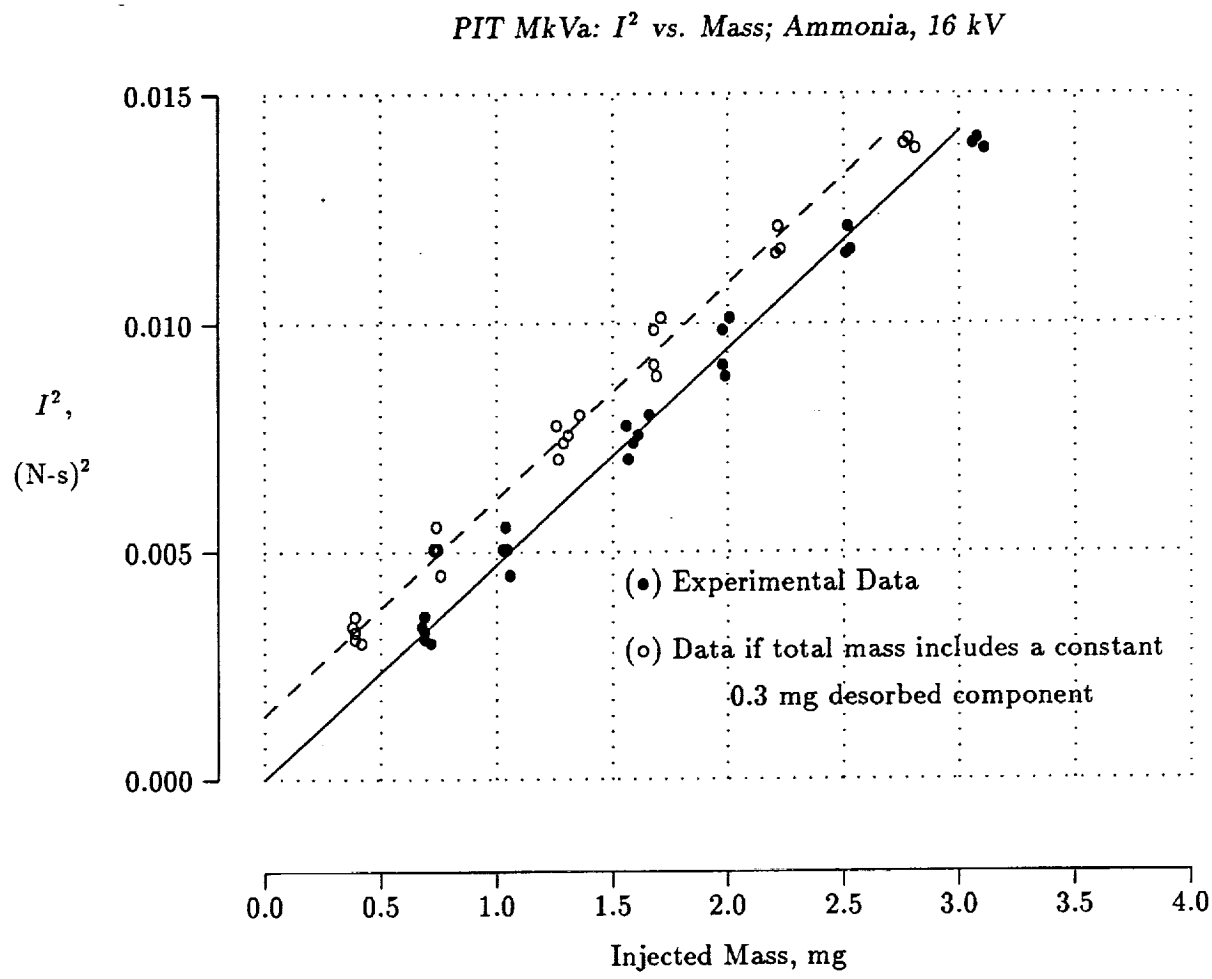
PIT MkVa: I^2 vs. Mass; Ammonia, 16 kV
0.015
0.010
0.005
0.000
I^2,
(N-s)^2
(•) Experimental Data
(o) Data if total mass includes a constant
0.3 mg desorbed component
0.0
0.5
1.0
1.5
2.0
2.5
3.0
3.5
4.0
Injected Mass, mg

Fig.D-2

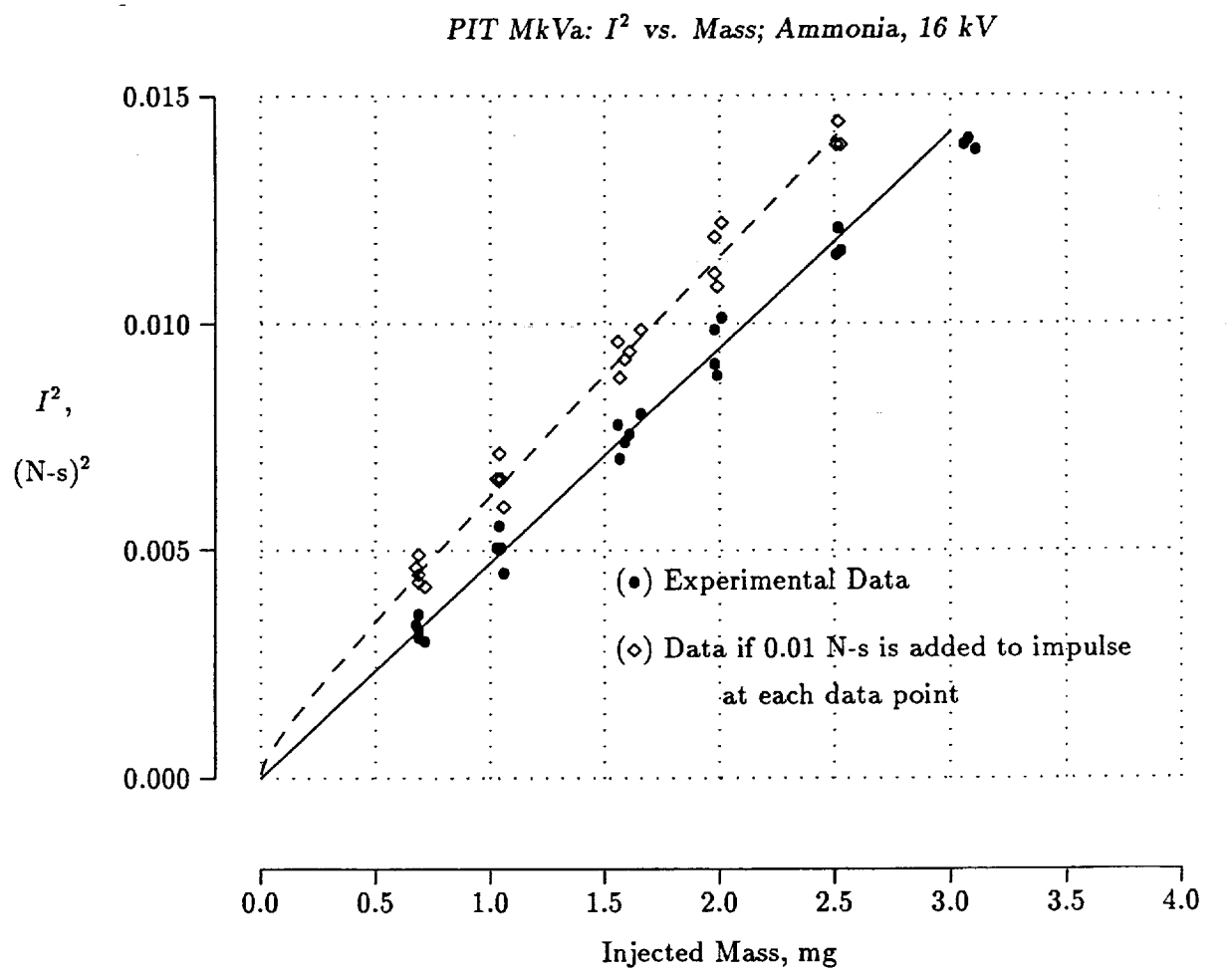
PIT MkVa: I^2 vs. Mass; Ammonia, 16 kV
0.015
0.010
0.005
0.000
I^2,
$(N\text{-}s)^2$
(•) Experimental Data
(◇) Data if 0.01 N-s is added to impulse at each data point
0.0
0.5
1.0
1.5
2.0
2.5
3.0
3.5
4.0
Injected Mass, mg

Fig.D-3

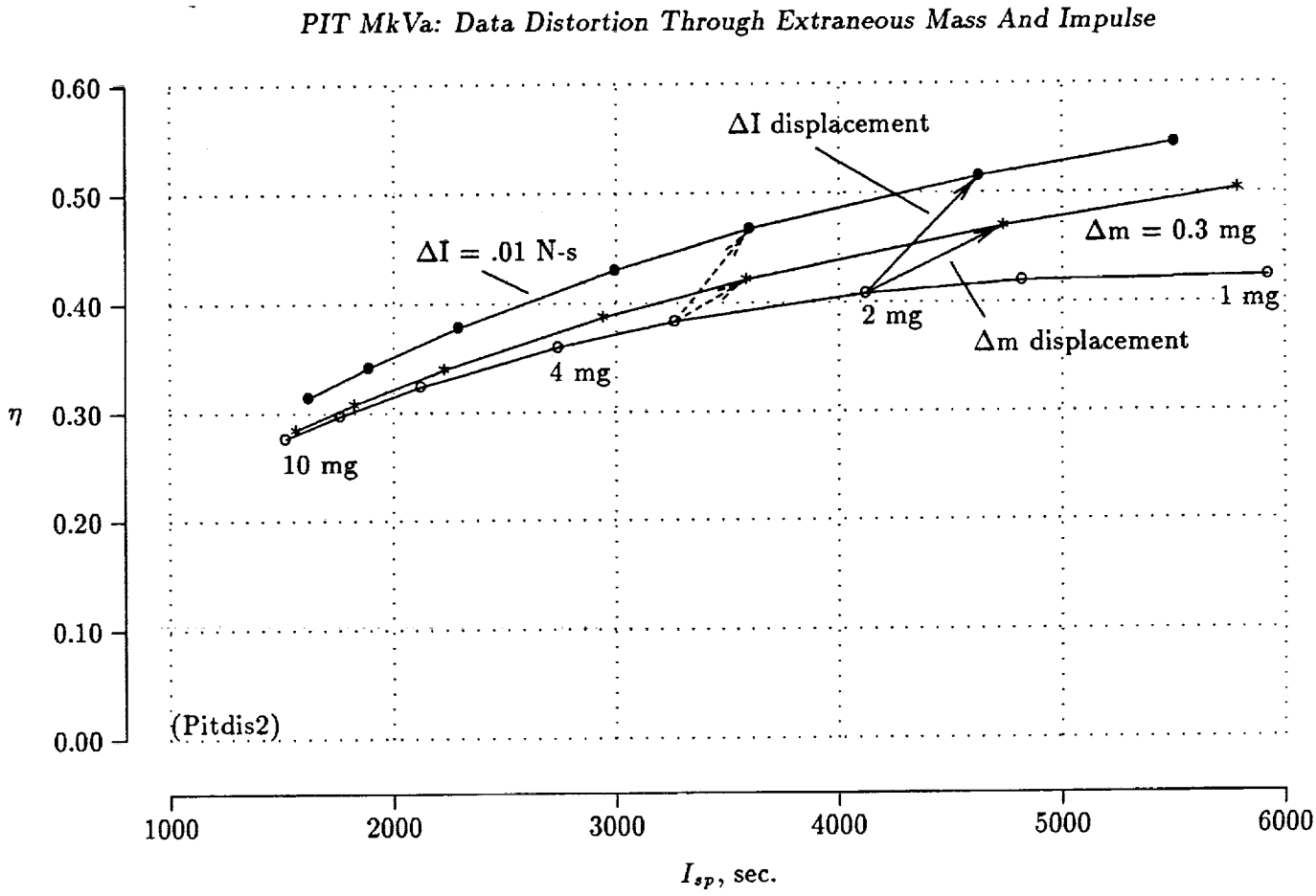
PIT MkVa: Data Distortion Through Extraneous Mass And Impulse
0.60
0.50
0.40
0.30
0.20
0.10
0.00
η
ΔI displacement
ΔI = .01 N-s
Δm = 0.3 mg
1 mg
2 mg
Δm displacement
4 mg
10 mg
(Pitdis2)
1000
2000
3000
4000
5000
6000
I_{sp}, sec.

Fig.D-4

REPORT DOCUMENTATION PAGE

Form Approved
OMB No. 0704-0188

1. AGENCY USE ONLY (*Leave blank*)	2. REPORT DATE	3. REPORT TYPE AND DATES COVERED
	July 1993	Final Contractor Report

4. TITLE AND SUBTITLE

The PIT MkV Pulsed Inductive Thruster

5. FUNDING NUMBERS

WU-506-42-42
C-NAS1-19291

6. AUTHOR(S)

C. Lee Dailey and Ralph H. Lovberg

7. PERFORMING ORGANIZATION NAME(S) AND ADDRESS(ES)

TRW Space & Technology Group
One Space Park
Redondo Beach, California 90278

8. PERFORMING ORGANIZATION REPORT NUMBER

E-7941

9. SPONSORING/MONITORING AGENCY NAME(S) AND ADDRESS(ES)

National Aeronautics and Space Administration
Lewis Research Center
Cleveland, Ohio 44135-3191

10. SPONSORING/MONITORING AGENCY REPORT NUMBER

NASA CR-191155

11. SUPPLEMENTARY NOTES

C. Lee Dailey, TRW Space & Technology Group, One Space Park, Redondo Beach, California 90278, and Ralph H. Lovberg, University of California, San Diego, California 92037. Responsible person, Project Manager, Michael LaPointe, Space Propulsion Technology Division, (216) 433-7453.

12a. DISTRIBUTION/AVAILABILITY STATEMENT

Unclassified - Unlimited
Subject Category 20

12b. DISTRIBUTION CODE

13. ABSTRACT (*Maximum 200 words*)

The pulsed inductive thruster (PIT) is an electrodeless, magnetic rocket engine that can operate with any gaseous propellant. A puff of gas injected against the face of a flat (spiral) coil is ionized and ejected by the magnetic field of a fast-rising current pulse from a capacitor bank discharge. Single shot operation on an impulse balance has provided efficiency and I_{sp} data that characterize operation at any power level (pulse rate). The 1-m diameter MkV thruster concept offers low estimated engine mass at low powers, together with power capability up to more than 1 MW for the 1-m diameter design. A 20 kW design estimate indicates specific mass comparable to Ion Engine specific mass for 10,000 hour operation, while a 100,000 hour design would have a specific mass 1/3 that of the Ion Engine. Performance data are reported for ammonia and hydrazine. With ammonia, at 32 KV coil voltage, efficiency is a little more than 50% from 4000 to more than 8000 seconds I_{sp}. Comparison with data at 24 and 28 kV indicates that a wider Isp range could be achieved at higher coil voltages, if required for deep space missions.

14. SUBJECT TERMS

Electric propulsion; Magnetoplasmadynamics; Inductive coupling

15. NUMBER OF PAGES

52

16. PRICE CODE

A04

17. SECURITY CLASSIFICATION OF REPORT	18. SECURITY CLASSIFICATION OF THIS PAGE	19. SECURITY CLASSIFICATION OF ABSTRACT	20. LIMITATION OF ABSTRACT
Unclassified	Unclassified	Unclassified	